Molecular Simulations of the Transport of Molecules across the Liquid/Vapor Interface of Water

Bruce C. Garrett* and Gregory K. Schenter

Chemical Sciences Division, Pacific Northwest National Laboratory, Richland, Washington 99352

Akihiro Morita

Department of Computational Molecular Science, Institute for Molecular Science, Okazaki 444-8585, Japan

Received October 17, 2005

Contents

1. Introduction

The transport of molecules across the liquid/vapor interface of water is a fundamental process that is important in a number of areas of science. Uptake of trace molecules by aqueous droplets is important in the atmosphere, as it enables new heterogeneous chemical pathways that are not available in the gas phase.[1−4] The uptake of molecules by water and partitioning to the air/water surface is important in aquatic environmental systems.[5] In addition, uptake is interesting because it is an example of a multiscale process in which the role of molecular processes at the air/water interface is not fully understood at this time.

Uptake of molecules by water droplets is a macroscopic process that is controlled by mass transport in the gas and liquid phases and can be influenced by molecular-scale processes occurring at the vapor/liquid interface. Careful experimental studies have provided important data on uptake rates of a variety of molecules by aqueous liquids. Reviews of experimental methods and results are available.[3,6−8] Earlier work[9,10] was focused on SO_2 uptake because of its importance in acid rain. Studies of the uptake of atmospherically important sulfur and nitrogen compounds abound.[11−19] There are also studies of atmospherically important oxidants (*e.g.*, OH, O_3, and HO_2)[12,19−21] and a number of studies of the uptake of organic species[22−28] and halide containing compounds.[11,17,29] A special case of uptake is the condensation of water on aqueous droplets.[30−33] These macroscopic measurements provide information about uptake by droplets that are micron size or larger and over time scales that are on the order of milliseconds or longer. For these time and length scales, the diffusion equation, which describes the evolution of the spatial probability distribution of the trace molecule toward an equilibrium distribution, adequately predicts mass transport in the liquid phase. The diffusion equation is not always a sufficient description of gas-phase mass transport, and treatment of the coupled evolution of spatial and velocity distributions (*e.g.*, as described by the Boltzmann equation) can be necessary to accurately describe mass transport near the interface.[34]

Understanding molecular-scale processes at the vapor/liquid interface involves dynamics of molecules over short distances, *e.g.*, nanometer (nm = 10^{-9} m) length scales, and short times, *e.g.*, nanosecond (ns = 10^{-9} s) time scales. Although these dynamical processes are difficult to probe experimentally, they can be followed explicitly in molecular simulations. Conversely, molecular simulations are currently limited to simulation sizes typically less than millions of molecules over nanosecond time scales, and therefore, they

* Corresponding author. E-mail: bruce.garrett@pnl.gov.

10.1021/cr040370w CCC: $59.00
Published on Web 03/09/2006

Bruce C. Garrett was born in Fort Knox, KY (1951), and received a B.S. in chemistry from the University of California, Irvine (1973), and a Ph.D. from the University of California, Berkeley (1977). He was a postdoctoral research specialist at the University of Minnesota from 1977 to 1979, a member of the scientific staff at Battelle Columbus Laboratories from 1979 to 1980, and cofounder of a small contract research company, Chemical Dynamics Corporation (Columbus, OH), where he conducted basic research from 1980 to 1989. He joined Pacific Northwest National Laboratory in 1989, became a Laboratory Fellow in 1994, and is currently Chemical Sciences Division Director at Pacific Northwest National Laboratory. His research interests include theories of chemical reactions, with focus on the effects of molecular environment (liquids, solids, and interfaces) on chemical reaction rates, molecular theories of gas-to-particle nucleation, and molecular simulations of molecular processes at aqueous interfaces. He is a Fellow of the American Physical Society and a Fellow of the American Association for the Advancement of Science.

Gregory K. Schenter was born in Boulder, CO (1961), and received a B.S. in physics from the California Institute of Technology (1983) and a Ph.D. from Cornell University (1988). He joined Pacific Northwest National Laboratory in 1988. His research interests include the role of quantum mechanics on chemical reaction rates, theories of nucleation, and molecular simulation techniques.

Akihiro Morita was born in Kamakura, Japan, in 1964. He received B.Sc. and M.Sc. degrees from the University of Tokyo and a Ph.D. in chemistry from Kyoto University in 1995 with Prof. Shigeki Kato as his advisor. He was a research fellow of the Japan Society for the Promotion of Science in 1992 and a research associate/assistant professor at Kyoto University from 1992 to 2003. He was also a research associate at the University of Colorado from 1999 to 2000, working with Prof. Casey Hynes. He moved to the Institute for Molecular Science in 2004 and has been an associate professor at the IMS since then. His research interests center on electronic structure and molecular dynamics in solutions and at liquid interfaces, including theories of interfacial mass transfer and nonlinear optical spectroscopy.

cannot directly address the macroscopic uptake process, which would require treating system sizes of several orders of magnitude more molecules over time scales that are at least 10^3 to 10^6 times longer. Consequently, understanding how molecular-scale processes at the vapor/liquid interface influence uptake requires an accurate multiscale model of the uptake process, *i.e.*, one that correctly integrates the physics at the different scales to bridge both length and time scales from molecular-level to macroscopic processes.

The most widely used approach to correlate and interpret uptake experiments is the resistance model of uptake,[3,7,35] which builds on the formulation of "characteristic process times" by Schwartz.[36,37] The resistance model is an approximate, continuum-level description of uptake, which includes continuum models of mass transport in the gas and liquid phases. The effects of interfacial processes that may impede the uptake process are introduced through a phenomenological parameter, the mass accommodation coefficient. This phenomenological model is distinct from an accurate multiscale model, which would explicitly couple the mathematical equations for molecular-scale processes with those for continuum-level processes. Nonetheless, it is sometimes possible to extract underlying details from careful analysis of macroscopic observations. For example, information about the temperature dependence of thermal rate constants provides information about reaction energetics. In a similar spirit, analysis of the mass accommodation coefficient has been used to infer details of molecular-scale interfacial processes from uptake experiments. The main conclusion from the analysis of these experiments is that the transfer of hydrophilic molecules across the vapor/liquid interface of water is an activated process.[38] The reliability of this conclusion about a molecular-scale process depends on a consistent means of relating the physics on a molecular scale to the physics on a continuum level.

Conclusions about the molecular-scale processes inferred from the uptake experiments have been tested using molecular-scale simulations. The simulations have consistently shown no evidence of an intrinsic activation barrier to molecules entering the liquid phase. The reliability of predictions from molecular simulations is determined largely by the accuracy of the representation of the intermolecular interaction potentials and the fidelity of statistical mechanics simulations of interfacial processes. The disagreement between the inferences from experimental observations of macroscopic processes and the observation of molecular processes from simulations of the air/water interface provides an opportunity for greater understanding of the important process of uptake. First, this disagreement demands a better knowledge of the reliability and limits of applicability of both the macroscopic model of uptake and the interaction potentials and models used in the molecular simulations. Second, a thorough understanding of the influence of molecular-scale processes on uptake requires an accurate

multiscale model that explicitly couples the molecular and continuum equations. One major purpose of this paper is to provide a review of molecular simulations of the vapor/liquid interface of water with an eye toward assessing the reliability of their predictions. Another major purpose is to address the issues of the reliability of the resistance model of uptake and the quantitative accuracy of experimental analyses. Derivation of molecular-level information from the macroscopic uptake experiments requires careful calibrations, as we discuss below, and we hope to indicate directions for future work that are needed to fully understand the reliability of the experimental analyses. The development of an accurate multiscale model is beyond the scope of this work and will not be discussed in any detail.

One purpose of this review is to provide a perspective on molecular-scale simulations and to evaluate the level of accuracy they provide for interfacial properties, particularly those associated with the uptake of molecules at the surface. In section 2, we briefly review computational methods commonly used in studies of aqueous interfaces, including functional forms of the molecular interaction potentials, descriptions of the simulation methodologies, and descriptions of the molecular models of the interface. In section 3, we present the results of simulations of select properties of the air/water interface and properties of molecular interactions at interfaces. Section 4 presents an overview of modeling approaches to the macroscopic process of uptake. In particular, we present a detailed description of the uptake process in flow tube experiments with the help of fluid dynamics calculations toward critical comparison between the uptake experiments and the molecular simulations. Section 5 provides concluding remarks.

2. Computational Methods

Reviews of simulations of aqueous interfaces are available.[39,40] The focus of the present work is on the vapor/liquid interface of water and on the results of simulations rather than the methodology. We provide brief summaries of the computational approaches used, and direct interested readers to the reviews for more detailed descriptions.

2.1. Interaction Potentials

A variety of interaction potentials have been used in simulations of the air/water interface, including ST2,[41] central force water (CFW),[42] MCY,[43] TIP4P,[44] CC,[45] SPC,[46] SPC/E,[47] two flexible versions of the SPC potential (SPC/F[46]and SPC-F[48]), NCC,[49] the Sprik−Klein model (SK),[50] POL3,[51] and the Dang−Chang model (DC).[52] These potentials are analytical functional forms, which, with the exception of CFW, SPC/F, and SPC-F, treat the water molecule as rigid. The ST2, CFW, TIP4P, SPC, SPC/E, SPC-F, SK, POL3, and DC models are empirical; that is, the parameters are adjusted so that classical simulations reproduce some set of experimental properties of the liquid phase. The MCY, CC, and NCC potentials were fitted to reproduce *ab initio* electronic structure information for small water clusters. Most of these potentials were developed to reproduce either bulk properties of water or the energetics of small water clusters, and their ability to reproduce properties of the air/water interface is a test of how well they extrapolate to conditions for which they were not parametrized. More recently, simulations of the air/water interface have been performed using the Car−Parrinello (CP) approach,[53] in which the molecular interactions are described using density functional theory (DFT).[54] The CP approach requires considerably more computational resources, so that only limited studies of properties of aqueous interfaces have been performed. Calculations have not been done yet with the CP approach to study properties relevant to mass transport. Therefore, we do not discuss this approach further in this review.

The total potential energy of a collection of water molecules for the ST2, MCY, TIP4P, CC, SPC, and SPC/E models is given by a pairwise additive form

$$U = \sum_{i<j} U_{ij}^{2B} \tag{1}$$

where the sum is over pairs of molecules in the system. The two-body term is generally expressed as the sum of a term accounting for short-range repulsive interactions and long-range attractive interactions arising from dispersion interactions and a term accounting for attractive and repulsive Coulombic interactions. For simplicity, we denote the former term as a Lennard-Jones interaction ($U^{LJ}_{\alpha_i,\beta_j}$), although a range of functional forms is used in practice. With the Coulombic interaction denoted Coulombic ($U^{C}_{\alpha_i,\beta_j}$), the two-body potential is given by

$$U_{ij}^{2B} = \sum_{\alpha_i,\beta_j} \left[U^{LJ}_{\alpha_i,\beta_j} + U^{C}_{\alpha_i,\beta_j} \right] \tag{2}$$

where α_i and β_j are sites on molecules i and j, respectively. The number and location of sites used to describe these interactions also vary for the different interaction potentials. The Coulombic interactions are determined by charges on the sites, which are treated as parameters in the model. The NCC, SK, POL3, and DC models add many-body interactions through a polarization term. The number of polarizable sites and their location varies in these models. Table 1 presents a summary of the different characteristics for some of these models, including the number of interaction sites. LJ, C, and P refer to "Lennard-Jones" type, Coulombic, and polarization interactions, respectively.

The flexible SPC models have the same characteristics as the SPC and SPC/E models (number of R, C, and P sites), and the equilibrium geometries have the same OH bond length and HOH bond angle. The central force water model is significantly different from the previously discussed analytical models. In the CFW model, the molecular geometries are not fixed and all atoms interact will all other atoms in the system through pairwise additive terms for HH, OH, and OO interactions. More complex functional forms are used than the usual Coulombic interactions plus "Lennard-Jones", although Coulombic interactions (*i.e.*, $\propto r^{-1}$) are included. The charges underlying the Coulombic terms give rise to a dipole moment of 1.86 D.

Empirical potentials are generally fitted to reproduce experimental condensed-phase properties such as the average potential energy $\bar{U}$, structural factors such as radial distribution functions, and pressure (for fixed volume simulations) or density (for fixed pressure simulations). Table 1 presents computed values for a few selected bulk properties: $\bar{U}$, the diffusion coefficient D, and the dielectric constant ϵ. Computed results are taken from the literature for ST2,[41] CFW,[42] MCY,[43,55] TIP4P,[44,56,57] CC,[45] SPC,[46,57] SPC/E,[47,57] NCC,[49,58] SK,[50,155] POL3,[51] and DC,[52] and are compared with experimental results.[59] Except for the MCY potential, which is fitted to *ab initio* data, the computed values of $\bar{U}$ are all

Table 1. Characteristics of Water Models and Selected Liquid Properties

	monomer properties						liquid properties[a]		
model	r_{OH} (Å)	θ_{HOH} (deg)	LJ sites	C sites	P sites	μ (D)	$\bar{U}$ (kJ/mol)	D ($\times 10^{-5}$ cm^2/s)	ϵ
ST2[41]	0.96	105	1	4[b]	0	2.35	−37.4[c]	1.9[c]	
CFW[42]	0.9584	104.45				1.86	−39.7	1.1	34[e]
MCY[43]	0.9572	104.5	3	3[d]	0	2.19	−35.6		34[e]
TIP4P[44]	0.9572	104.52	1	3[d]	0	2.18	−41.6	3.3[57]	61[57]
CC[45]	0.9572	104.5	3	3[d]	0		−39.0		
SPC[46]	1	109.47	1	3	0	2.27	−37.7	3.6[57]	72[57]
SPC/E[47]	1	109.47	1	3	0	2.35	−41.4	2.4[57]	70[57]
NCC[49]	0.9572	104.5	4[f]	3[d]	2[g]		−44.6	2.5	100[58]
SK[50]	0.9572	104.52	1	3[d]	1[h]	1.85	−42.2		130−140[155]
POL3[51]	1	109.47	1	3	1[i]	1.85	−43.6	3.1	
DC[52]	0.9572	104.52	1	3[d]	1[i]	1.85	−41.2	2.1	
exp[59]	0.9572	104.52				1.85	−41.5	2.4	78

[a] Temperature and density are 298 K and 0.997 g/cm^3, and results are from the model reference unless noted otherwise. [b] Coulombic interaction sites on H atoms and tetrahedral sites 1.0 Å from an O atom. [c] $T = 283$ K. [d] Coulomb sites on H atoms and M site. [e] $T = 292$ K. [f] Lennard-Jones type interaction on all atoms plus M site. [g] Point dipoles on OH bonds. [h] Distributed charge model centered on M site. [i] Point dipole on M site.

within about 4 kJ/mol (or 10%) of the experimental value. The diffusion coefficient is a more critical test of many of these potentials, and it shows more deviation from the experimental results, differing by over a factor of 2 for CFW.

Simulations of molecules interacting with the vapor/liquid interface of water require intermolecular interaction potentials for the molecule−water interaction as well as the water−water interaction. Simulations of the interaction of solute molecules with the vapor/liquid interface of water have been performed for methanol,[60−62] ethanol,[63−66] ethanediol,[66] decanol,[67] phenol,[68,69] *p*-*n*-pentylphenol,[70] dimethyl sulfoxide (DMSO),[71] acetonitrile,[62] benzene,[72] ammonia,[73] hydroxyl radical (OH),[74−77] hydroperoxyl radical (HO_2),[76] hydrogen peroxide (H_2O_2),[76] ozone (O_3),[74,76,77] O_2,[76] N_2,[76] CO_2,[78] and SO_2.[78] These simulations have typically employed all-atom, empirical models such as Amber,[79] CHARMM,[80] and OPLS[81] force fields to describe the intramolecular potentials. In these models, bond lengths are generally constrained while intramolecular bends and torsions are treated explicitly. Interactions between the solute and water molecules typically include long-range dispersion and short-range repulsion (*e.g.*, Lennard-Jones) as well as Coulombic interactions between fixed atomic charges. Partial charges on atoms in the solute molecules are fitted to reproduce the electrostatic potential from electronic structure calculations using approaches such as CHELPg.[82] The parameters for the long-range dispersion and short-range repulsion interactions are typically determined by the Lorentz−Bertholot mixing rules.[83] In a few cases,[72−75,77] polarizable force fields are used, and for DMSO,[71] a flexible (but nonpolarizable) force field was employed.

2.2. Simulation Methods

We provide here a review of simulation methods used to probe the energetics, dynamics, and kinetics of adsorbate molecules interacting with aqueous liquid interfaces, which is the main focus of this work. The general prescription for simulation of these types of systems is as follows. Molecular dynamics (MD) simulations are performed on a system consisting of a solute and hundreds to thousands of water molecules in a rectangular simulation cell in which the *z* axis is elongated (see Figure 1). For example, for a simulation of 500 water molecules, dimensions of 2.5 nm × 2.5 nm × 7.5 nm have been used.[84] The slab of water forms two

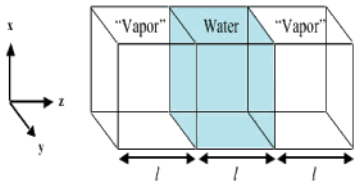

Figure 1. Schematic of simulation cell. A slab of water occurs between two vapor sections. The *z* axis is perpendicular to the two free water surfaces.

interfaces with the "vapor" phase. The "vapor" is usually void of molecules, because the sample size is small and the probability of evaporation of a water molecule is low. For example, the probability of finding a water molecule in the "vapor" represented by a cube with side 2.5 nm is 1% at room temperature. Similarly, the average number of air molecules (*e.g.*, O_2 and N_2) in a cube this size at room temperature is 0.4. Therefore, treating the "vapor" as a vacuum is a reasonable approximation in this case.

Simulations are performed at a constant volume and temperature, typically with periodic boundary conditions applied in all three directions. Use of 3D periodic boundary conditions can lead to artificial structuring of solvent or solute molecules induced by interactions between periodic replicas of the slabs. Both truncation and Ewald summation of the long-range (*e.g.*, Coulombic) interactions have been employed in the literature. If long-range interactions are truncated, then the separation between slabs just needs to be larger than the truncation distance to avoid these problems. Treating long-range interactions by Ewald summation presents more of a challenge. The computational costs of 3D Ewald summation become more expensive as the interslab separation becomes larger in an effort to decrease interactions between slabs. Ideally, it would be best to employ 2D periodic boundary conditions that only impose periodic boundary conditions in the two dimensions parallel to the interface. However, implementing 2D Ewald summation is more difficult than the standard 3D approach, and it is usually not done. These issues become more of a problem when dealing with the solvation of charged species, particularly for studies of the interfaces of high concentration electrolyte solutions. These effects for the low concentrations (*e.g.*, one solute with hundreds of solvent molecules) of neutral species are expected to be much less important, although systematic studies of the effects have not yet been done.

2.2.1. Energetics of Solute Transport across the Gas/Liquid Interface

Free energy profiles for transfer of solute molecules across the interface are computed either using a constrained mean force approach,[85] statistical perturbation theory,[86] or umbrella sampling techniques.[39,87] The reaction coordinate for transfer is taken to be z_s, which is the separation distance of the z component of the center of mass of the solute molecule from the z component of the center of mass of the slab of water molecules. The potential of mean force (PMF) is defined in the constrained mean force approach as

$$W(z_s) = -\int_{z_0}^{z_s} \langle f_z(z_s') \rangle_{z_s'} \, dz_s' \quad (3)$$

where $f_z(z_s)$ is the z component of the total force exerted on the solute at z_s, and $\langle \cdots \rangle_{z_s}$ represents an average over a canonical ensemble of all coordinates with the value of z_s fixed. By definition, $W(z_s)$ is zero at $z_s = z_0$ and we choose z_0 as a value far from the interface where the force is zero (*i.e.*, in the bulk liquid or vapor phase). The PMF curve can also be constructed from free energy differences for two points along the reaction coordinate as given by

$$W(z_s + \Delta z_s) - W(z_s) = -RT \ln(\langle \exp\{-[U(z_s + \Delta z_s) - U(z_s)]/RT\} \rangle_{z_s}) \quad (4)$$

where R is the gas constant, T is the temperature, and $U(z_s)$ is the total potential (summed over all interactions in the system) with the center-of-mass separation fixed at z_s. The increment Δz_s must be sufficiently small so that the configurations sampled in the constrained average $\langle \cdots \rangle_{z_s}$ provide an adequate sampling of the potential at $z_s + \Delta z_s$. Finally, the PMF curve can be obtained from the probability distribution $P(z)$, which is the probability of finding the solute molecule at a location z_s along the reaction coordinate,

$$W(z_s) = -RT \ln\left[\frac{P(z_s)}{P(z_0)}\right] \quad (5)$$

where we again define $W(z_s) = 0$ at $z_s = z_0$. Simulations of $P(z_s)$ use a biasing potential that allows for sampling of high free energy (low probability) regions. A series of biasing potentials are used to give $P(z_s)$ for overlapping regions or "windows" of z_s, and the full PMF curve is constructed by requiring that $W(z_s)$ is a continuous function of z_s.

2.2.2. Kinetic Studies of Solute Transport

Some of the solute molecules are surface active; that is, their free energies at the interface are lower than their free energies in either the gas or liquid phases. For these systems, the dynamics of motion into the bulk phases from the interface requires surmounting an activation barrier, requiring long-time simulations to study these events. A convenient approach for activated processes is to use transition state theory (TST) to calculate the rate constants for escape of the solute molecule into the gas phase (desorption) or into the bulk liquid (absorption). TST was first used to describe evaporation and condensation over 50 years ago.[88] When classical mechanics is valid, TST can be derived by making one approximation, the fundamental dynamical assumption, which states that trajectories originating in reactants that reach the transition state dividing surface separating reactants from products will proceed to products without recrossing the dividing surface.[89] This approximation obviates the need to explicitly follow classical trajectories and allows the reaction rate constant to be expressed in terms of quasiequilibrium properties (*i.e.*, partition functions in the reactant and transition state regions). It has long been recognized that the TST rate constant can be expressed in terms of the potential of mean force,[90,91] and for the choice of reaction path used here, z_s, the rate constant is given by[92]

$$k^{\mathrm{TST}}(T) = \frac{k_B T}{h Q^{\mathrm{R}}(T)} \exp[-[W(z_s^{\ddagger}) - W_{\mathrm{surf}}]/RT] \quad (6)$$

where k_B is the Boltzmann constant, h is the Planck constant, $Q^{\mathrm{R}}(T)$ is the reactant partition function, $z_s^{\ddagger}$ is the value of z_s at the local maximum in the potential of mean force curve, and W_{surf} is the value of the PMF for the local interfacial minimum. In this case we are interested in the rate of escape from a local well at the interface either into the vapor (desorption) or into the bulk liquid (absorption), so that the reactant partition function is proportional to the configurational integral over the Boltzmann factor $\exp(-U/RT)$ where the configurations are constrained to a region for which the solute is in the local well at the interface. The PMF is related to configurational integrals as shown in eqs 3 and 4 in which the value of z_s is constrained to a single value. The partition function can therefore be obtained by an average over z_s in the region of the well:

$$Q^{\mathrm{R}}(T) = \sqrt{\frac{M k_B T}{2\pi\hbar^2}} \int_{\mathrm{well}} dz_s \exp[-(W(z_s) - W_{\mathrm{surf}})/RT] \quad (7)$$

where M is the mass of the solute molecule and $\hbar = h/2\pi$.

Equation 6 is used to calculate rate constants for both absorption $k_{\mathrm{absorb}}^{\mathrm{TST}}$ and desorption $k_{\mathrm{desorb}}^{\mathrm{TST}}$. Since the reactant state is the same for both processes, the ratio of the two rate constants can be expressed in terms of a free energy difference

$$\frac{k_{\mathrm{absorb}}^{\mathrm{TST}}}{k_{\mathrm{desorb}}^{\mathrm{TST}}} = \exp[-(\Delta W_{\mathrm{absorb}}^{\ddagger} - \Delta W_{\mathrm{desorb}}^{\ddagger})/RT] \quad (8)$$

where $\Delta W_{\mathrm{absorb}}^{\ddagger}$ and $\Delta W_{\mathrm{desorb}}^{\ddagger}$ are the maximum values of the potential of mean force between the interface and bulk liquid and between the interface and the vapor, respectively, measured relative to the potential of mean force at the interface minimum.

The fundamental dynamical assumption of transition state theory assumes that a trajectory with the solute at $z_s^{\ddagger}$ and a velocity directed toward products (*e.g.*, away from the interface) proceeds to product without recrossing $z_s^{\ddagger}$. However, it has long been recognized that the solvent can induce recrossings of the transition state dividing surface and that the recrossing can lead to errors in the TST rate constant.[93,94] Grote−Hynes theory[95] is a convenient approach to estimate the dynamical, or nonequilibrium, absorption rate constant. It approximates the dynamics of barrier crossing using a harmonic approximation to the potential of mean force at the top of the solute barrier and treats the effect of friction and random forces arising from solvent fluctuations by a generalized Langevin equation (GLE) with a friction kernel.

The absorption rate constant is approximated by

$$k_{\text{absorb}} \approx \kappa^{\text{GH}} k_{\text{absorb}}^{\text{TST}} \tag{9}$$

where the TST rate constant is given by eq 6. The Grote−Hynes transmission coefficient, κ^{GH}, for the GLE model reduces to the following analytical form

$$\kappa^{\text{GH}} = [\kappa^{\text{GH}} + \omega_{\text{b}}^{-1} \int_0^\infty \mathrm{d}t \exp(-\kappa^{\text{GH}} \omega_{\text{b}} t) \zeta(t;z^{\ddagger})]^{-1} \tag{10}$$

where ω_{b} is the barrier frequency for the potential of mean force and $\zeta(t;z^{\ddagger})$ is the kernel for solvent friction on the reaction coordinate at the barrier maximum. The solvent friction kernel can be calculated from the force−force correlation function via

$$\zeta(t;z_0) = \left(\frac{1}{Mk_{\text{B}}T}\right) \langle \delta F(t;z_0) \delta F(0;z_0) \rangle_{z_0} \tag{11}$$

where $\delta F(t;z)$ is the instantaneous force on the reaction coordinate (*i.e.*, in a direction perpendicular to the liquid/vapor interface) for a given solvent configuration. The ensemble average is over all solvent configurations and internal and orientational degrees of freedom of the solute, in which the center of mass separation z_s is kept fixed at z_0.

2.2.3. Dynamical Simulations of Solute Transport

Direct simulation of the dynamics of uptake is a convenient approach to probe the factors controlling transport across the interface, particularly when barriers are low and the motion in the liquid phase is diffusive. Two types of dynamical simulations related to transport of solute molecules across the interface have been performed. The first is used to obtain the probability that solute molecules stick to the surface upon impact from the gas phase. In these studies classical dynamics is used to follow trajectories of solute molecules that begin in the vapor phase, in a region where $W(z_s)$ is nearly constant. Initial configurations and velocities for the water molecules in the slab are chosen from an equilibrium simulation of the water interface (with no solute present), and the incident molecule is given an initial random orientation. The initial center of mass velocity of the incident molecule is taken from a Maxwell distribution in which only those velocity vectors headed toward the surface are included.

The second type of dynamical simulation is used to examine the dynamics of solute molecules that are equilibrated at the interface. In this case initial configurations and velocities for both the water and solute molecules are chosen from an equilibrium simulation of the water interface with the solute present. For the systems studied in this manner, the time scales for escape from the interface, either by desorption into the vapor or adsorption into bulk, are long compared to the time scale for equilibration of the solute molecule at the interface. After initial equilibration, much longer trajectories are computed to obtain the probability of finding the solute molecule at a location z_s.

3. Results of Molecular Simulations

We are mainly concerned with the dynamics and kinetics of solute molecules at the air/water interface, particular as these processes are related to uptake of solute molecules by the liquid. These processes are strongly influenced by the dynamics of water molecules at the interface. One issue is the relationship between the dynamics of interfacial water molecules, which are typically followed over nanosecond time scales in molecular simulations, and the dynamics of molecular collisions with the surface and evaporation from the surface. At 298 K the gas-phase pressure of water vapor is 24 Torr and the collision rate of water molecules with the liquid surface is about 10^{23} collisions $\text{cm}^{-2}\ \text{s}^{-1}$. The average volume of a water molecule in bulk water is about $(0.3\ \text{nm})^3$; therefore, the collision rate is about 1 collision per molecular area every 10 ns. Thus, the processes of evaporation and condensation do not play a significant role in molecular simulations, which are typically limited to nanosecond time scales. We will return to this issue when we discuss kinetics of molecular uptake below.

3.1. Interfacial Properties of Water

Since the properties and processes of aqueous interfaces can strongly influence molecular uptake, we first focus on molecular simulations of the vapor/liquid interface of water. Almost 30 years of molecular simulations of liquid/vapor interfaces have provided detailed information about the structure, energetics, and dynamics of the interface and molecules on the liquid surface. Numerous investigators using a variety of intermolecular interaction potentials have performed many simulations of the interface of water.[39,84,96−100] Figure 2 shows a representative snapshot from a molecular simulation of the liquid/vapor interface of water using the SPC/E potential, which is adapted from the work of Taylor *et al.*[84] Although the quantitative results vary from study to study, a consistent qualitative picture emerges from this body of work:

(1) The transition from vapor to liquid is over molecular length scales. The average density goes from the bulk liquid value to the vapor value over a distance of 0.3−0.6 nm.

(2) The interface is rough on molecular length scales (see Figure 2). Although the average density smoothly varies across the interface, snapshots of molecular configurations show variations in the height of individual molecules that have the greatest extension into the vapor.

(3) The interface fluctuates on a time scale of picoseconds ($\text{ps} = 10^{-12}$ s). Irregular features on the interface are created and disappear on the time scale of a few picoseconds.

(4) Time scales for molecular events at the interface are short (on the order of a few picoseconds). For example, the time scale for interchange of water molecules on the surface with those below the surface is on the order of a few to several picoseconds.

The adequacy of simulation methods and water interaction potentials that are used for calculations of interfacial properties and processes can be evaluated by comparison with experimental results. Surface sensitive spectroscopic methods[101] have provided valuable information about molecular orientation and hydrogen bonding at the interface. The results from these experimental studies do not provide conclusive tests of common simulation results because considerable analysis is generally needed to extract quantities that can be directly compared with simulations. Alternatively, more sophisticated simulation techniques are needed to calculate the experimentally observed quantities directly. An example of this type of approach is the theoretical analysis of Morita and Hynes[102] for simulating sum frequency generation spectra. Recently, results of these types of modern surface sensitive experiments have been used to question the validity of simulation methods and particularly intermolecular po-

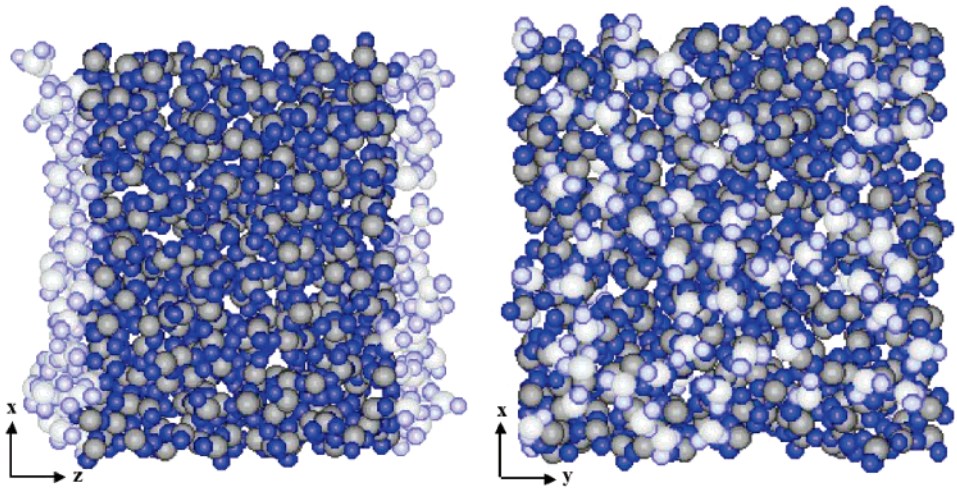

Figure 2. Snapshot of a simulation of the air/water interface using the SPC/E potential at room temperature. The left panel shows a side view of the two interfaces, which are perpendicular to the *z* coordinate, and the right panel shows a top view of one of the interfaces. The lighter colored water molecules are in the region of the interface where the average density drops below 90% of its bulk value.

tentials for aqueous systems.[103] As stated above, we do not believe these results provide conclusive tests of the simulation methods. As an example, X-ray studies of water microjets led to the conclusion that the interface is dominated by hydrogen bonding configurations in which the interfacial water molecules participate in two acceptor-only hydrogen bonds (the H bonds are between the O atoms on the surface waters and protons on subsurface waters).[104] These studies used action spectroscopies, observing ion and electron yield from the surface upon X-ray absorption. The ejected ions (*e.g.*, H^+) preferentially come from water molecules at the surface and thus provide a probe of the interface. These experiments were interpreted as showing evidence that the orientation and hydrogen bonding of water molecules at the interface are different than those observed in molecular simulations. However, there is no current theory that links the observed action spectra with molecular structure at the interface and it is not clear whether the distribution of orientations of water molecules at the interface is equally sampled by this technique. It seems likely that this type of spectroscopy only samples those water molecules with H atoms oriented into the vapor. In other words, this experimental technique may not "see" the molecular orientations that are most probable in the molecular simulations. Therefore, it is not valid to use this type of experimental observable to make general claims about the validity of water interaction potentials, as has been done recently.[103]

A more quantitative test of molecular simulations of aqueous interfaces is the surface tension, for which experimental values as a function of temperature are well-known.[105] A review of surface tension calculations and the differences in simulation methods is provided by Alejandre and Tildesley.[100] Table 2 and Figure 3 present a comparison of calculated values[48,52,60,65,97−100,106−108] of surface tension for various water models with experimental values.[105,107] Although there is variation for the different interaction potentials, many of the more commonly used potentials (*e.g.*, TIP4P, SPC/E, and DC) yield values that are within about 30% of the experimental value. It is noted that the early calculations of surface tension (*e.g.*, for the ST2 potential[106]) used a different technique to compute the surface tension than is typically used in more recent calculations. In addition, the simulation protocol used (*e.g.*, number of molecules in the simulation and treatment of long-range interactions) can affect the calculated results. The SPC/E potential has been studied extensively, and comparison of the results by Alejandre and Tildesley[100] with those of Taylor *et al.*[84] shows that the effects of simulation size and treatment of long-range interactions change the surface tension by less than 10%. The SPC/E potential also provides accurate reproduction of the temperature dependence of the surface tension.

Another property often reported from simulations is the interfacial width. In simulations, this quantity is uniquely defined as the distance between the location where the average density is 10% of the bulk value and the location

Table 2. Comparison of Calculated and Experimental Values of the Surface Tension of Water (γ)[a]

model	γ (dyn/cm)	model	γ (dyn/cm)
ST2	97 ± 6[106]	SPC/E	65.0 ± 3.0[65]
MCY	23.7 ± 3.4[99]	SPC/E	69.5 ± 3.0[107]
TIP4P	132 ± 46[97,b]	SPC−F	123.6[48]
TIP4P	∼50[60,c]	POL3	55 ± 6[108]
CC	30.5 ± 2.7[98]	DC	92 ± 5[52]
SPC/E	66.0 ± 3.0[100,d]	exp	72[105]

[a] Temperature is 298 K unless noted otherwise. [b] $T = 325$ K; experimental value is 68 dyn/cm at this temperature. [c] $T = 300$ K. [d] $T = 328$ K; experiment value is 65 dyn/cm at this temperature.

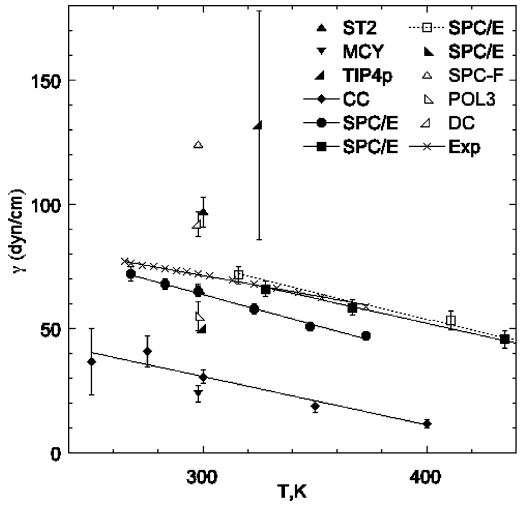

Figure 3. Surface tension of water as a function of temperature. Experimental values (denote by × symbols) are compared with calculated values using different interaction potentials for water.

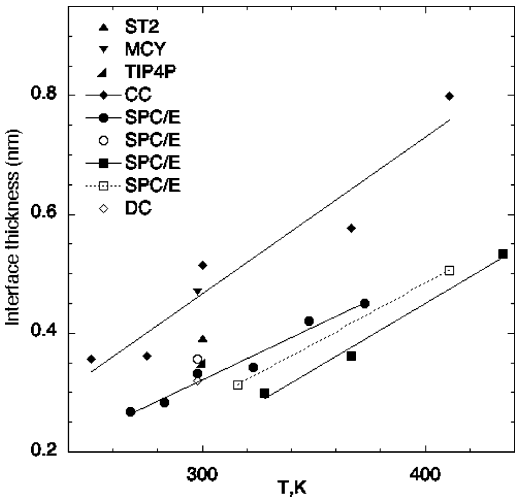

Figure 4. Calculated interfacial thickness as a function of temperature for different water models.

where it is 90% of bulk. Figure 4 provides a summary of the temperature dependence of this quantity. Values for different interaction potentials vary by as much as 60−70%, but the more commonly used potentials are in good agreement with each other. Experimental measures of this width are about a factor of 2 larger, ranging from 0.7 to 1.8 nm from room temperature to 350 K.[109] This difference has been attributed to the lack of capillary waves in the simulations.[98]

Several investigators have also calculated the surface potential of water.[69,71,110−112] In addition, two reviews of theoretical and experimental determination of surface potentials have appeared recently.[113] Although calculation of the surface potential is straightforward, direct comparison with experimentally derived values is complicated because electrochemical evaluations require measurements on finite dilution electrolyte solutions and it is difficult to separate contributions from the ions in the solution from those from the pure solvent.[110,112] For this reason we do not elaborate on this property and refer the interested reader to the reviews of computational approaches provided by Pratt[110] and Sokhan and Tildesley.[112]

3.2. Molecular Properties and Processes at the Air/Water Interface

Molecular simulations provide a wealth of information about the structure, energetics, and dynamics of solute molecules at the air/water interface. Figure 5 shows an example of a snapshot of a hydrophilic solute molecule, ethanediol, at the air/water interface. The snapshot displays the propensity of the alcohol to orient the OH groups downward into the water, leaving the aliphatic part outside above the water. In this section we focus on simulations that provide an understanding of molecular scale processes that can impede uptake at the air/water interface. Although the rate of passage through the interface is the most important property, we first focus on the energetics that control molecular uptake and then discuss studies of the kinetics and dynamics of uptake.

3.2.1. Energetics of Solute Transport across the Gas/Liquid Interface

Calculations of free energies of absorption and adsorption have been used to evaluate the accuracy of the molecular interactions used in simulations of uptake. Experimental free energies of solvation are available for a number of solute molecules,[20,114−117] and free energies of adsorption at the interface are also available for a few solute molecules.[68,115,118−120] Figure 6 provides an example of a calculated potential of mean force, in this case for ethanol uptake.[65,66] The zero of energy for $W(z_s)$ is chosen to be in the bulk liquid, *i.e.*, at $z_s \ll 0$, where we define $z_s = 0$ at the interface. The PMF goes through a small barrier, $W_{barrier} = 1.6$ kJ/mol, upon approaching the interface from the bulk liquid, then goes into a well, $W_{surf} \approx -6$ kJ/mol, at the interface, and finally rises monotonically from the well to the value in the vapor phase, $W_{vapor} \approx 24$ kJ/mol. The quantities needed to calculate the rate constant ratio given in eq 8 are energies measured relative to the minimum energy at the interface. These are the barrier from the well into the bulk, which is given by $\Delta W^{\ddagger}_{absorb} = W_{barrier} - W_{surf} \approx 7.5$ kJ/mol, and the barrier from the well into the vapor, which is given by $\Delta W^{\ddagger}_{desorb} = W_{vapor} - W_{surf} \approx 30$ kJ/mol.

Figure 6 also defines free energy quantities that allow a test of the calculations against experiment. The value of the solvation free energy ΔG_{solv} is just the difference in the potential of mean force between bulk liquid and vapor. With the zero of energy of the PMF chosen to be in the bulk liquid, $\Delta G_{solv} = W_{vapor}$. The free energy of adsorption can also be computed from the PMF but is obtained from the difference of energies in the bulk region, where the PMF is constant, and at the interface, where it is has a well. The free energy of adsorption requires accounting for the bound states in the interface well. The free energy difference between adsorption

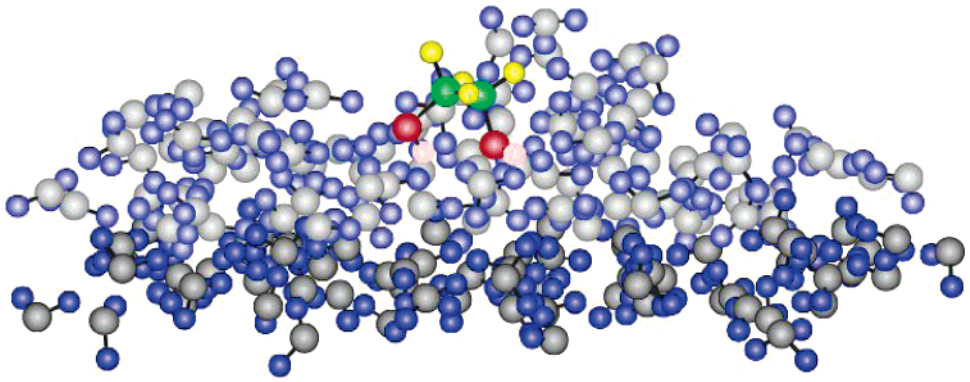

Figure 5. Snapshot of a simulation of ethanediol at the air/water interface using the SPC/E potential at room temperature. The coloring of the water molecules is the same as in Figure 2. Carbon atoms, aliphatic H atoms, O atoms, and H atoms in the OH group of the alcohol are green, yellow, red, and white, respectively.

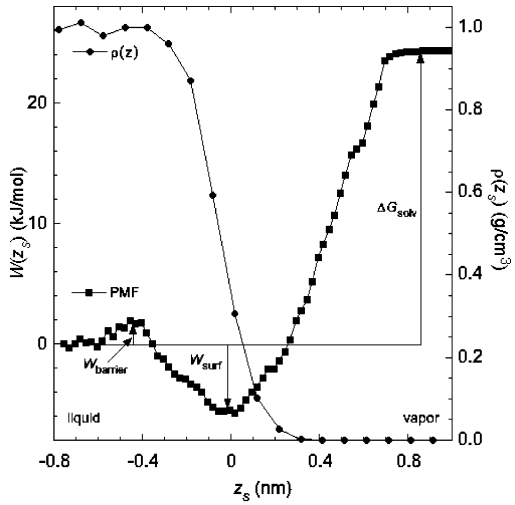

Figure 6. Potential of mean force for ethanol transfer across the liquid/vapor interface of water (filled squares) as a function of distance perpendicular to the water interface. Water density is also shown as a function of distance perpendicular to the water interface. Free energy quantities are described in the text.

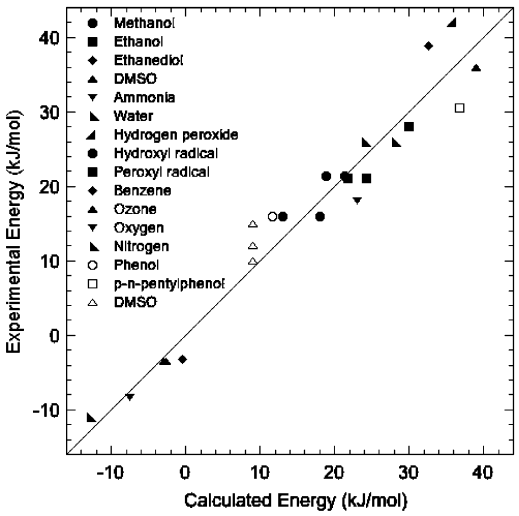

Figure 7. Comparison of experimental and calculated free energies of solvation (filled symbols) and of adsorption (open symbols) for several solute molecules.

at the interface and bulk solvation is given by

$$\Delta G_{\mathrm{surf}} = W_{\mathrm{surf}} + G^{\mathrm{R}} = W_{\mathrm{surf}} - RT \ln Q^{\mathrm{R}} \qquad (12)$$

where Q^{R} is defined in eq 7. Note that the reactant partition function Q^{R} is defined with the energy relative to the minimum of the interfacial well, W_{surf}. The integral in eq 7 for the reactant partition function is over the well region, which in Figure 6 should extend over the region $z_s \approx -0.4-0.4$ nm. The contribution to the free energy from Q^{R} can be estimated for the case shown in Figure 6 by approximating $W(z_s)$ as a parabola. For this system, $W(z_s)$ can be fitted to a harmonic potential with a frequency of about 100 cm^{-1}. At 298 K, Q^{R} has a value of about 2 and its contribution to ΔG_{surf} is about 0.8 kJ/mol. We can expect contributions from Q^{R} to the free energy of adsorption to be a few kilojoules per mole or less for the systems studied here. As a first approximation, the values of ΔG_{surf} reported below neglect this contribution.

Table 3 and Figure 7 present a comparison of computed[62,64−68,70−73,75−77] and experimental[20,114−120] values of ΔG_{bulk} and ΔG_{surf}. The filled symbols in Figure 7 are for ΔG_{bulk} (the free energy difference between vapor and bulk liquid), while the open symbols are for $-\Delta G_{\mathrm{surf}}$ (the free energy difference between bulk liquid and the interface). For the wide range of interaction potentials used in these calculations, the agreement with experiment for both ΔG_{bulk}

Table 3. Free Energies of Solvation (ΔG_{solv}), Free Energies of Adsorption at the Surface (ΔG_{surf}), and Barrier Heights in the Potential of Mean Force Occurring between Bulk Liquid and the Interface (W_{barrier})[a]

		ΔG_{solv}		ΔG_{surf}[b]		W_{barrier}
solute	water model	calc	exp	calc	exp	calc
methanol	SPC/E[47]	18.8[62]	21.3[114]	−8.4[62]		<2[c]
	TIP4P[44]	21.3[64]	21.3[114]	−2.9[64]		<2[d]
ethanol	SPC/E[47]	24.3[65,66]	21.1[114]	−5.9[65,66]		1.6[65,66]
	TIP4P[44]	21.8[64]	21.1[114]	−5.0[64]		<2[d]
ethanediol	SPC/E[47]	32.6[66]	38.9[114]	−5.4[66]		1.6[66]
decanol	SPC/E[47]			−39.7[67]		8.8[67]
phenol	TIP4P[44]			−11.7[68]	−15.9[f]	2.1[68]
p-*n*-pentylphenol	TIP4P[44]			−36.8[70]	−30.5[118]	∼3[g]
DMSO	SPC/F[46]	39[71]	36[115]	−9[71]	−10[119], −12[115], −15[120]	∼0[e]
acetonitrile	SPC/E[47]	18.2[62]		−4.8[62]		<2[c]
benzene	DC[52]	−0.4[72]	−3.2[114]	−16.3[72]		<3[h]
ammonia	DC[52]	23[73]	18[114]	0[73]		0[73]
water	DC[52]	28[73]	26[114]	0[73]		0[73]
	SPC/E[47]	24[76]	26[114]	<1[76]		0[76]
OH	POL3[51]	13[75,77]	16[20,117]	−4.6[75,77]		0[75,77]
	SPC/E[47]	18[76]	16[20,117]	−5.9[76]		0[76]
HO_2	SPC/E[47]	28[76]	28[116]	−3.3[76]		<1[76]
H_2O_2	SPC/E[47]	42[76]	36[116]	−1.5[76]		0[76]
ozone	POL3[51]	−2.6[77]	−3.5[116]	−4.2[77]		0[77]
	SPC/E[47]	−2.9[76]	−3.5[116]	−4.8[76]		<1[76]
O_2	SPC/E[47]	−7.5[76]	−8.4[116]	−1.9[76]		<1[76]
N_2	SPC/E[47]	−13[76]	−11[116]	−4.2[76]		<1[76]

[a] The free energies ΔG_{surf} and W_{barrier} are relative to solvation in the bulk liquid. All energies are kJ/mol. [b] ΔG_{surf} is approximated by W_{surf}. Errors from this approximation are in the range 1−4 kJ/mol (see text). [c] Figure in work by Paul and Chandra[62] shows barrier less than ∼2 kJ/mol. [d] Figure in work by Wilson and Pohorille[64] shows barrier less than ∼2 kJ/mol. [e] Figure in work by Benjamin[71] shows barrier <1 kJ/mol. [f] Eisenthal as reported by Pohorille and Benjamin.[68] [g] Figure in work by Pohorille and Benjamin[70] shows barrier of about 3 kJ/mol. [h] Figure in work by Dang and Feller[72] shows barrier less than ∼3 kJ/mol.

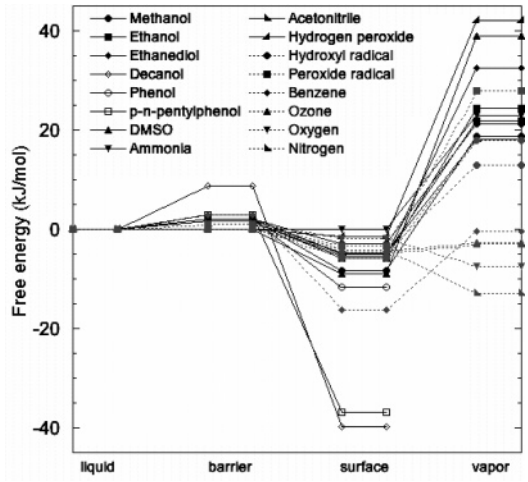

Figure 8. Schematic of potential of mean force curves for several solute molecules. The zero of energy is taken as the value of the PMF in bulk liquid. Values for the barrier, interfacial well, and gas phase are depicted.

and ΔG_{surf} is uniformly good. The largest errors in ΔG_{bulk} are for the molecules with the largest values—about 6 kJ/mol for ethanediol and H_2O_2. Similarly, the largest error for ΔG_{surf} is also for the system with the largest value—about 6 kJ/mol for *p*-*n*-pentylphenol. For the hydrophilic systems, the errors are less than about 20% for the free energies. DMSO is the one system for which there are values for ΔG_{bulk} and ΔG_{surf} for both experiment and theory. The calculated value of ΔG_{bulk} overestimates experiment by about 3 kJ/mol, and the calculated value of ΔG_{surf} is within 1 kJ/mol of the experimental range. The conclusion from a review of this information is that the interaction potentials are capable of reproducing energetic quantities to within several kilojoules per mole for a wide range of systems (from hydrophilic to hydrophobic, including radical species) and to within 20% of the free energy values for hydrophilic species.

Table 3 also presents values of the barrier in the potential of mean force $W_{barrier}$. The largest value occurs for the system with the deepest minimum at the interface—decanol gives a value of 8.8 kJ/mol. Another system with a deep surface minimum is *p*-*n*-pentylphenol, but its barrier is only about 3 kJ/mol. This finding is consistent with the free energy profile for ethanol shown in Figure 6. Figure 8 summarizes the computed potentials of mean force tabulated in Table 3. Values of the PMF are shown for the barrier, well, and vapor, relative to the bulk liquid. For all the hydrophilic molecules, the free energy for removing the molecule from the interface to the vapor is greater than the free energy barrier for going into liquid. As shown in Figure 8, this finding is general, reproduced in a variety of computed results[62,64−68,70−73,75−77] for a variety of solute molecules using a variety of interaction potentials for water and solute−water interactions (see Table 3 for references).

3.2.2. Kinetic Studies of Solute Transport

Substituting the values for $\Delta W^{\ddagger}_{desorb}$ and $\Delta W^{\ddagger}_{absorb}$ for hydrophilic molecules into eq 8 predicts that absorption rate constants are larger than desorption rate constants; that is, $k^{TST}_{absorb}/k^{TST}_{desorb} > 1$. This finding is in opposition to the analysis of uptake experiments that have led to the conclusion that the desorption rate constants should be larger. The disagreement between the simulated values for the relative kinetics and the experimental implications for these values has led to studies that examine dynamical effects that are missing in a simple transition state theory approach, which is the basis for eq 8.

One method to include dynamical effects in TST is to use Grote−Hynes theory,[91,93] which has been applied to the kinetics of solute uptake by water in two cases in the literature.[66,67] Taylor *et al.*[66] have shown that the solvent friction effects are negligible in the region of the PMF controlling the desorption rate constant, and the dynamical effects only need be included for the absorption rate constant. Grote−Hynes theory approximates the effects of dynamical recrossings of the transition state dividing surface, which decrease the rate constant. For ethanol the multiplicative Grote−Hynes factor κ^{GH} is 0.12,[66] while for decanol it is 0.046.[67] The effect on the absorption rate constant can be effectively included by shifting the free energy of activation $\Delta W^{\ddagger}_{absorb}$ by the factor $-RT \ln(\kappa^{GH})$. The free energy shifts are 5.3 and 7.6 kJ/mol for ethanol and decanol, respectively. This magnitude of energy shift is not large enough to make the ratio $k^{TST}_{absorb}/k^{TST}_{desorb}$ less than 1 for the hydrophilic solute molecules. For ethanol this ratio of rate constants is reduced from about 9×10^3 to 10^3 with the inclusion of the Grote−Hynes factor.

3.2.3. Dynamical Simulations of Solute Transport

Dynamical studies have been used to examine two effects that can lead to lower apparent uptake of solute molecules. The first effect is reflection of solute molecules incident on the air/water interface. These types of calculations have been performed for ethanol,[64] methanol,[61] HO_2,[121] OH,[75,77] O_3,[77] and water.[77,108,122,123] The results of these studies are summarized in Table 4. The more recent studies by Roeselova, Vieceli, and co-workers[75,77] analyzed the trajectories for deflection, scattering, desorption, adsorption, and absorption of the incident molecule. A deflected trajectory encounters a repulsive interaction at a relatively large distance from the surface and returns to the gas phase, while a scattered trajectory makes a single, intimate contact with the surface before returning to the gas phase. The probabilities for these two events are combined in Table 4. Desorption also leads to return of the molecule to the gas phase, but after initial sticking to the interface. Earlier studies did not distinguish between the different channels that result in the incident molecule returning to the gas phase. The probability of loss to the gas phase is time dependent, since there is a finite probability of desorption of adsorbed molecules, so that the probably of loss to the gas phase increases as the length of the trajectory increases. Vieceli *et al.*[77] provided a nice analysis of how to obtain a time-independent molecular mass accommodation coefficient from the trajectories. That analysis was not performed for the results shown in Table 4, and the desorption probabilities in Table 4 are reported for the time limit of the trajectories as indicated in the table. Surface-active species (those with minima in the PMF at the interface) can stay resident at the interface for a long period of time before either absorbing into the bulk liquid or desorbing into the gas phase. For some of the studies it was not determined whether the molecules that did not return to the gas phase were adsorbed at the surface or absorbed into the bulk. In these cases, the reported value represents the sum of probabilities for these two events, which can be interpreted as a sticking probability.

Except for ozone, the largest probabilities are for adsorption or absorption and the sticking probability is in the range

Table 4. Results of Scattering Calculations for Molecules Incident upon the Interface of Water[a]

		trajectory		probability (%)			
molecule	water model	time (ps)	total no.	reflected	desorbed	adsorbed	absorbed
ethanol[64,b]	TIP4P[44]	20	1000		1.8	98.2[c]	
methanol[61]	SPC[46]	100	500		0.2	99.8[c]	
HO_2[121,d]	MCY[43]	10, 20[e]	500		0.6	99.4[c]	
OH[75,77]	POL3[51]	90	250	6.0	4.8	56.8	32.4
O_3[77]	POL3[51]	90	250	12	64	20	4
H_2O[77,108]	POL3[51]	90	250	<1	0	16	84
H_2O[122]	SPC/E[47]	10−100	1000		0.3	99.7[c]	

[a] Temperature is 298 K unless noted otherwise. [b] $T = 310$ K. [c] Adsorption and absorption channels are not distinguished. [d] $T = 293$ K. [e] Half the incident HO_2 molecules were followed for 10 ps, and the other half were followed for 20 ps.

89−100% at temperatures near room temperature. Nagayama and Tsurata[123,124] also used molecular dynamics simulations on the SPC/E and CC potentials to calculate the sticking probability of water on water interfaces over the temperature range 330−550 K and found the sticking probably decreased from 99% to 54% as temperature increased. Similarly, Ishiyama *et al.*[125] performed MD simulations on the TIP3P potential[44] and obtained very similar results. Although sticking becomes <1 for high temperatures, it is 1 for temperatures below about 330 K. The results for ozone are unique because it is hydrophobic. As shown in Table 3 and Figure 8, ozone's free energy of solvation is uphill in energy from the gas phase and, therefore, it is more likely for an ozone molecule resident at the surface to desorb than absorb.

The picture that emerges from these studies is that liquid water is very efficient at dissipating the translational energy of the incident molecule, leading to rapid equilibration of the majority of the incident molecules. After a relatively short period of time (on the order of tens of picoseconds), the probabilities of desorbing and absorbing are determined by the kinetics of the evaporation and absorption processes. This picture of rapid equilibration of molecules at the liquid/vapor interface of water is general, being reproduced for four different water models and six incident molecules, as summarized in Table 4.

The second effect is preferential desorption from the surface, as opposed to absorption into the bulk, over time periods much longer than tens of picoseconds. This effect was studied by molecular simulations of solute molecules initiated at the interface. Wilson and Pohorille[64] calculated a 30 ns trajectory at 310 K with ethanol initially at the liquid/vapor interface. The trajectory was observed to move into the bulk, and the average probability of finding the ethanol molecule in the bulk was appreciable. The time dependent distribution or probability of finding ethanol at location z, $p(z,t)$, obtained from simulations was compared with the solution to the forced-diffusion or Smoluchowski equation

$$\frac{\partial p(z,t)}{\partial t} = D\frac{\partial^2 p(z,t)}{\partial z^2} + \frac{D}{kT}\frac{\partial}{\partial z}\left[p(z,t)\frac{\partial W}{\partial z}\right] \qquad (13)$$

where D is the diffusion coefficient for the molecule in water and W is the PMF. [Equation 13 can be generalized to account for a z-dependent diffusion constant. The relation between detailed molecular motion and approximate descriptions such as eq 13 continues to be an active area of research. For an estimate of the position dependence of diffusion coefficients, see ref 126. These studies indicate that diffusion is faster in the interfacial region and the bulk diffusion coefficient is recovered when the average density attains its bulk value (*e.g.*, about 0.5 nm from the interface for water at room temperature).] The agreement between the molecular simulations and the forced-diffusion equation was excellent, indicating that the rate of entry of ethanol into water from the interface is diffusion limited. In addition, during the 30 ns trajectory the ethanol molecule never escaped into the gas phase.

A similar study was performed for DMSO on water by Benjamin[71] with similar conclusions. Comparison of results from molecular simulations with those from a forced-diffusion equation indicated that the time scale in the molecular simulations for the process of mass transport from the interface into bulk is the same as that given by the forced-diffusion equation. The results for ethanol and DMSO are consistent with an experimental study that clearly demonstrated the mass transport of decanol to obey a diffusion-controlled mass transfer model for systems that are sufficiently dilute.[127] The study of ethanol led Wilson and Pohorille[64] to state that "the mechanism by which an ethanol molecule becomes solvated can therefore be described as capture by the interface with almost unit probability followed by diffusion on the equilibrium free energy surface."

3.3. Summary

The structure (*e.g.*, density profiles and molecular orientation), energetics (*e.g.*, free energy profile, surface tension, and surface potential), and dynamics (*e.g.*, gas/surface collisions and bulk liquid/surface exchange) have been studied by many investigators for a variety of molecules at water's vapor/liquid interface. The quantitative results vary from study to study, but the qualitative trends are similar. In particular, all calculations of free energy profiles for moving a solute molecule from the gas phase to the surface and into the bulk indicate that almost all the small hydrophilic molecules which have been studied to date are surface active (*i.e.*, their free energy at the interface is lower than that in the bulk) and that the free energy profiles exhibit only small intrinsic barriers (typically less than 5 kJ/mol) for moving the solute from the bulk liquid to the interface. Based on these studies, the general conclusion is that the absorption rate is larger than the desorption rate, *i.e.*, $k_{absorb} > k_{desorb}$, which contradicts the interpretation of uptake experiments.[38,103,128] Molecular simulations of dynamical processes for solute molecules at the interface are consistent with the kinetic studies—absorption is faster than desorption.

The MD simulations do not include collisions of other vapor molecules, particularly water molecules, with the surface that could affect the dynamics of solute uptake. We can estimate time scales of absorption and desorption and compare them to collision processes that are described at the beginning of section 3. By using the computed energetics of the mass transport process, the potentials of mean force

(PMFs), with transition state theory, rate constants for desorption into the vapor and absorption into bulk liquid can be approximated. Lifetimes of the solute molecule to desorption and absorption are given by the reciprocals of these unimolecular rate constants. For ethanol, these values are 70 ns for τ_{desorb} and 0.1 ns for τ_{absorb}, where the absorption lifetime includes the Grote−Hynes correction factor. The time scale for diffusional motion of ethanol in water can be estimated from $\tau_{diff} = l^2/D$, where l is a characteristic length scale and D is the diffusion coefficient. The diffusion coefficient for ethanol in water is about 7×10^{-5} cm^2 s^{-1} so that the diffusional time scale for molecular length scales (l = 0.3−0.6 nm) is about 0.01−0.05 ns. The lifetime of the activated absorption process, τ_{absorb}, is longer than the diffusional lifetime, τ_{diff}; therefore, τ_{absorb} sets the lifetime of about 0.1 ns for an ethanol molecule on the surface. As discussed above, the collision rate of vapor-phase water molecules with the molecules on the surface at ambient conditions is about 1 collision every 10 ns. Therefore, the dynamics of solute molecules interacting with the surface should not be affected by collision of water molecules with the surface.

4. Modeling Uptake

While molecular dynamics simulations provide a straightforward means to study interfacial mass transfer dynamics at a molecular level, it is a very challenging problem to compare on the same footing the molecular-scale information thus obtained with the kinetic measurements by heterogeneous uptake experiments.[2,7] This difficulty arises because the phenomenological uptake kinetics is controlled by coupled transport in the gas and liquid phases and at the interface. Accordingly, careful analysis is indispensable to derive intrinsic information on interfacial mass transfer from observed transport phenomena. This section briefly summarizes recent investigations of uptake experiments toward meaningful comparison with molecular simulations.

4.1. Uptake Coefficient and Resistance Model

In molecular dynamics studies, the microscopic interfacial mass transfer rate is defined by the sticking probability α',

$$\alpha' = \frac{\text{number of molecules adsorbing or absorbing into the liquid}}{\text{number of molecules impinging from the gas into the surface}} \quad (14)$$

$$(0 \le \alpha' \le 1)$$

On the other hand, the observed mass transfer rate in uptake experiments is represented by the uptake coefficient γ, a widely used parameter for atmospheric applications.[1,2] The latter is defined as the net deposition flux from gas to liquid, normalized by the maximum collision flux per unit surface area given by the quantity $c_0\bar{v}/4$, where c_0 is the concentration in the bulk gas phase and $\bar{v} = (8k_BT/\pi M)^{1/2}$ is the mean molecular velocity. α' and γ are the dimensionless parameters for mass transfer efficiency, in the molecular and phenomenological senses, respectively. Determining the relation between these two quantities is an ultimate goal for the analysis of heterogeneous kinetics.

The uptake coefficient γ involves gas-phase diffusion, transport across the interface, and liquid-phase diffusion coupled with chemical reaction.[37] The most widely used scheme of heterogeneous kinetics is given by the resistance model,[7] which decouples the observed rate into elemental steps in the gas, interface, and liquid as follows:

$$\frac{1}{\gamma} = \frac{1}{\Gamma_g} + \frac{1}{\alpha} + \frac{1}{\Gamma_{sol} + \Gamma_{rxn}} \quad (15)$$

where the inverse of γ is given the interpretation of an overall resistance for mass transport and the three terms on the right-hand side correspond to resistance in the gas ($1/\Gamma_g$) and liquid [$1/(\Gamma_{sol} + \Gamma_{rxn})$] and at the interface ($1/\alpha$). All the rate constants in eq 15, *i.e.*, Γ_g, Γ_{sol}, Γ_{rxn}, and α, are normalized by $c_0\bar{v}/4$ and are dimensionless. Equation 15 assumes that the overall transport consists of serial, multistep processes whose kinetic rate constants are independent.

An important parameter in describing gas-phase transport is the Knudsen number Kn, which is equal to the ratio of the mean free path of molecules in the gas phase to the droplet radius. There are different expressions for $1/\Gamma_g$ over the diffusive regime ($Kn \ll 1$) and the transition regime ($Kn \sim 1$), although these formulas generally provide similar results.[1] The most widely used formula for analyzing uptake experiments is given by Fuchs and Sutugin,[129]

$$\frac{1}{\Gamma_g} = \frac{0.75 + 0.283Kn}{Kn(1 + Kn)}, \quad Kn = \frac{6D_g}{d\bar{v}} \quad (16)$$

where D_g is the diffusion coefficient in the gas phase and d is the droplet diameter. In the diffusive limit ($Kn \to 0$), $1/\Gamma_g$ becomes

$$\frac{1}{\Gamma_g} \to \frac{d\bar{v}}{8D_g} - 0.467 \approx \frac{8D_g}{d\bar{v}} - \frac{1}{2}, \quad (Kn \to 0) \quad (17)$$

The last expression can be directly derived from the Smoluchowski diffusion equation,[130] assuming a spherical gaseous concentration field around the droplet. (The term $^1/_2$ comes from the kinetic collision correction at the boundary.[131])

The third term of eq 15 including Γ_{sol} and Γ_{rxn} assumes that the liquid-phase transport and the chemical reaction occur in parallel in the liquid phase. By solving the diffusion-reaction equation in the liquid phase,[132] the third term is represented as

$$\Gamma_{sol} + \Gamma_{rxn} = \frac{4HRT}{\bar{v}}\left(\sqrt{\frac{D_l}{\pi t}} + \sqrt{D_l k}\right) \quad (18)$$

where H is the Henry constant for the solute, R is the gas constant, D_l is the diffusion coefficient in the liquid, and k is the (pseudo-) first-order rate constant in the liquid. In many cases of liquid-phase reactions after uptake, the rate constant for reactions with a trace amount of solute is reasonably described as pseudo-first-order. Note that the solubility term Γ_{sol} is time dependent, $\sim t^{-1/2}$, describing transient transport before reaching saturation.

4.2. Mass Accommodation Coefficient

In the resistance formula of eq 15, the second term $1/\alpha$ should account for interfacial resistance. α is called the mass accommodation coefficient, referring to the normalized flux across the gas/liquid interface. In the coupled diffusion equations for multiphase transport, α is introduced in the

Table 5. Experimental Mass Accommodation Coefficients α of Soluble Species into Liquid Water[1,2]

gas	T (K)	α
SO_2	260−292	0.11,[10] 0.13 (298 K)[6,14]
HO_2	275	> 0.02,[20] >0.2[12]
H_2O_2	273	0.18[10]
N_2O_2	271−282	0.06−0.04[11]
HNO_3	268−293	0.19−0.07,[11] 0.11 (298 K)[6,14]
NH_3	290	0.097,[6,14] 0.04 (299 K),[16] 0.08[18]
CH_3OH	273	0.056[22]
HCHO	267	0.02[23]
CH_3CHO	267	0.03[23]
HCOOH	273	0.047[22]
CH_3COOH	273	0.067,[22] 0.19 (258 K)[26]
HCl	274−294	0.18−0.06,[11] 0.12[6]
CH_3SO_3H	273	0.13[15]
phenol	278−298	0.037−0.0066[28]
H_2O	258−280	0.32−0.17,[33] 0.006−1[32]
C_2H_5OH	273	0.048,[22] 0.100,[26] 0.0278 (273.8 K)[27]

boundary conditions for mass flux across the discontinuous interface.[133,134] Table 5 summarizes mass accommodation coefficients α of soluble solute molecules into water, reported by heterogeneous experiments.[6,10−12,14,15,18,20,22,23,26−28,32,33] It is noteworthy that the experimental values of α are generally <1. Even in very soluble species (an extreme case of which is water), α is on the order of 0.1, which might appear inconsistent with molecular dynamics simulations.

In connection to the resistance formula, some questions arise associated with the definition of α. First is the validity of the fundamental assumption of eq 15 to decouple the multistep processes. This assumption has been widely accepted for heterogeneous mass transport, essentially because of separation of the spatial and temporal scales for the transport processes. Gas-phase and liquid-phase transport occur in spatially distinct regions, and the diffusion coefficients in liquid and gas are usually separated by several orders of magnitude.[37] However, the validity of decoupling interfacial transport from diffusive transport in the gas and liquid phases is less evident. Assessment of the validity of this approximation requires quantitative considerations from a multiscale perspective, as mentioned in the Introduction. Equation 15 rather defines the parameter α based on the decoupling assumption.

The second question, closely related to the first one, is the relation between α and α′. They are both dimensionless parameters, commonly associated with mass transport efficiency at the gas/liquid interface. Despite their analogy, one should be cautious of equating α with α′. The two quantities have distinct origins in definitions; α is derived from the kinetic analysis of the uptake coefficient γ via eq 15, whereas α′ is directly defined from the surface scattering events in a molecular simulation. In fact, this apparent analogy has caused a great deal of confusion in the interpretation of uptake experiments. To distinguish the two, we call α the mass accommodation coefficient and α′ the sticking probability.

The third question is how the other terms in eq 15, Γ_g, Γ_{sol}, and Γ_{rxn}, are calibrated in the process of deriving α from γ. The calibration may depend sensitively on the derived value of α, when the gas- or liquid-phase resistance is substantial.[135] The use of eqs 16 and 18 to estimate the gas- and liquid-phase resistances, for example, involves idealized assumptions. In some cases the input parameters, such as the Henry constant, are not well-known. This calibration is an important but challenging issue under realistic conditions of uptake experiments, and is discussed next.

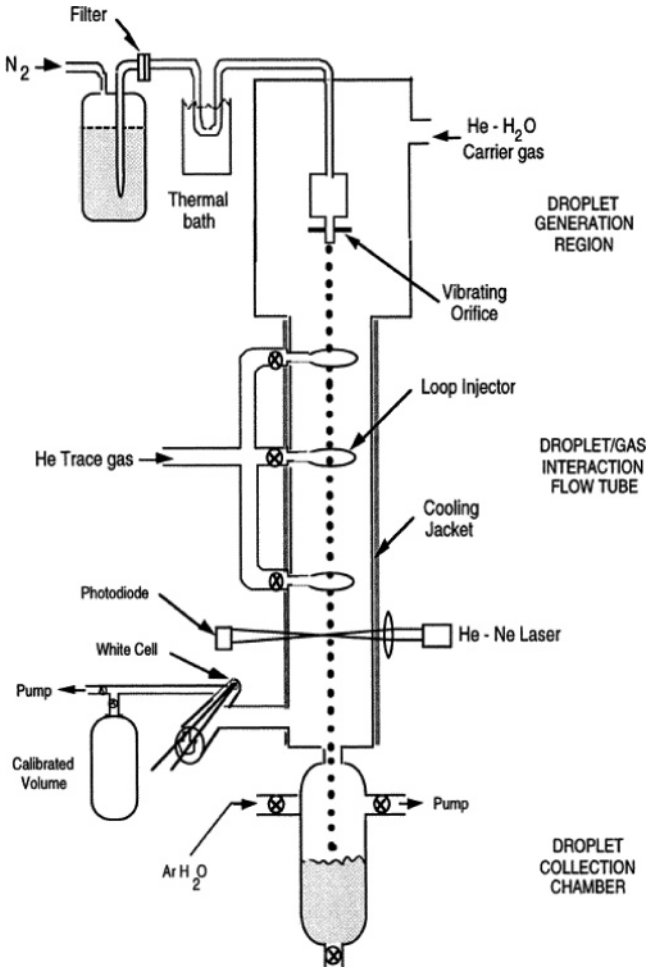

Figure 9. Schematic picture of the droplet train flow tube. (Reprinted with permission from ref 25. Copyright 1996 American Chemical Society.)

4.3. Uptake Measurement and Analysis

Uptake measurements have been carried out with a variety of experimental devices, including Knudsen cells, droplet train flow tubes, coated wall flow tubes, aerosol flow tubes, and impinging flows.[2,7] These techniques commonly derive the uptake coefficient γ by measuring the concentration change in the gas (or liquid) phase in contact with the interface under controlled conditions. A special case of uptake is condensation, where the solute species is the same as the liquid, and consequently, it is not straightforward to measure the concentration change. In this case, the net growth rate of droplets or films can be measured at a supersaturated condition.[30,32]

The droplet train flow tube has been extensively used to report a comprehensive set of mass accommodation coefficients of soluble species into water. This experimental technique has a number of practical advantages to focus on the mass accommodation process as discussed below. In this subsection we examine the droplet train flow tube approach in detail, as a representative example to compare with molecular simulations.

4.3.1. Droplet Train Flow Tube

A schematic picture of the droplet train apparatus is shown in Figure 9. It uses a highly controlled train of droplets passing through the low-pressure flow reactor.[7] The gas region in the flow tube contains a trace amount of solute

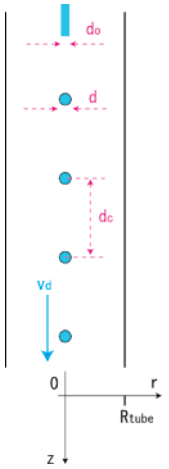

Figure 10. Geometric configuration of the droplet train flow tube.

species in saturated water vapor. A carrier gas such as He or Ar is used if necessary. The decrease in the gas-phase concentration is measured after contact with the droplet surfaces.

A vibrating orifice with a frequency f_0 generates a train of monodispersed droplets. As illustrated in Figure 10, the orifice diameter is assumed to be d_0, the droplet speed is v_d, the spacing between the droplet centers is d_c, and the volume flow rate of liquid is F_l. These parameters should satisfy the following geometric relation,

$$F_l = \frac{\pi}{6}d^3 f_0 = \frac{\pi}{4}d_0^2 v_d, \quad v_d = f_0 d_c \tag{19}$$

and consequently $d \sim f_0^{-(1/3)}$ and $d_c \sim f_0^{-1}$ at a constant F_l, indicating that a higher orifice frequency results in smaller droplets with a smaller spacing between droplets. The liquid surface area per unit flow tube segment, S, is therefore

$$S = \frac{\pi d^2}{d_c} = \left(\frac{3\pi^2}{4}\right)^{2/3} F_l^{-(1/3)} d_0^2 f_0^{1/3} \sim f_0^{1/3} \tag{20}$$

The decrease in solute concentration in the gas phase is usually analyzed under the plug flow model, which assumes the gas flow as radially uniform in the flow reactor and thereby allows a one-dimensional treatment of the gas flow along the axis. The axial dependence of the solute concentration $c(z)$ is given by the following differential equation,

$$\frac{dc(z)}{dz} = \frac{\bar{v}\gamma S}{4F_g}c(z) \tag{21}$$

where F_g is the gas volume flow rate and the concentration $c(z)$ is radially averaged over the cross section of the flow tube. Equation 21 is integrated along the axial interaction length L to give the uptake coefficient γ,

$$\gamma = \frac{4F_g}{\bar{v}SL}\ln\left(\frac{c(L)}{c(0)}\right) \tag{22}$$

The actual experimental apparatus can change the liquid surface area S by switching the orifice frequency f_0, and it can measure the variation in concentration. Accordingly, for two measured concentrations at the exit, $c_1(L)$ and $c_2(L)$, corresponding to two surface areas, S_1 and S_2, respectively, the uptake coefficient γ is given by

$$\gamma = \frac{4F_g}{\bar{v}(S_1 - S_2)L}\ln\left(\frac{c_1(L)}{c_2(L)}\right) \tag{23}$$

After obtaining the uptake coefficient γ, the mass accommodation coefficient α is derived from eq 15 with proper calibration.

4.3.2. Advantages and Problems

The experimental technique illustrated above has a number of advantages. (a) The total pressure is typically 5−20 Torr, and the droplet diameter d is tens to hundreds of microns.[7] Relatively low pressures and small droplets are utilized to suppress the gas-phase diffusive resistance $1/\Gamma_g$. (b) By changing the droplet speed v_d (typically tens of m/s) and the interaction length L (∼cm), the exposure time of the liquid surface can be controlled on the order of milliseconds. This short and controllable exposure time is a great advantage to evaluate the liquid-phase solubility resistance $1/\Gamma_{sol}$. (c) The liquid surface is constantly refreshed to minimize accumulation of surface impurities at the liquid surface. (d) Since the ambient gas contains a saturated vapor of the liquid, net condensation or evaporation of the droplets is suppressed in the flow tube. Therefore, mass transfer is effectively decoupled from heat transfer in the measurement.

Features (a) and (b) above allow this technique to be applied to the cases of relatively large α (hence small interfacial resistance $1/\alpha$), where the mass accommodation is not necessarily the rate determining step in the uptake process. In addition, features (c) and (d) offer simplified uptake conditions with little influence of surface impurity or nonequilibrium heat transfer. These advantages make this technique a unique experimental means to study mass accommodation of soluble species into water.

On the other hand, the analysis also poses a number of problems that need to be addressed. First, the uptake coefficient γ is derived using the one-dimensional eq 21 on the basis of the plug flow assumption. While the plug flow assumption is widely used to model flow tube experiments, its use for modeling the droplet train flow tube is more questionable because the running droplet train induces significant radial gradients of the concentration and velocity in the gas flow, as we illustrate below.

The second problem is the difficulty to assess the gas-phase resistance, as the actual uptake occurs into a train of running droplets in the gas flow. This situation is apparently different from the ideal situation of the Fuchs−Sutugin or Smoluchowski formulas, eq 16 or 17, which assume spherical boundary conditions around an isolated droplet in a quiescent gas field. The actual conditions in the flow tube are not amenable to analytical treatment, and thus experimental analysis has resorted to an empirical estimation, whose accuracy or reliability should be carefully examined.[136]

Third, the resistance in the liquid phase also deserves further investigation. One possible missing effect in the conventional uptake model of section 4.1 is convection within the liquid droplets. The moving droplets could cause internal convection through the shear interaction to the gas, which could enhance the liquid-phase transport of solute species into the inside of the droplets. While internal circulation was experimentally observed for falling water drops in clouds,[133] this shear interaction in the droplet train flow tube is expected to be less significant[137] because of the low pressure in the

flow tube and hydrodynamic coupling among the moving train of droplets. However, a quantitative understanding of the liquid convection effect remains unsolved in the uptake experiments. In the following section we focus on the first two problems associated with gas-phase transport in the flow tube.

4.4. Fluid Dynamics Analysis for Gas-Phase Transport

As discussed above, gas-phase transport in the droplet train flow tube should not be regarded as ideal diffusion as the original Fuchs−Sutugin formula assumes. To empirically account for gas-phase resistance in flow tube experiments, a modified Fuchs−Sutugin formula has been proposed and used,[138] where the Knudsen number in eq 16 is substituted with an effective quantity Kn^{eff}:

$$\frac{1}{\Gamma_g} = \frac{0.75 + 0.283Kn^{\mathrm{eff}}}{Kn^{\mathrm{eff}}(1 + Kn^{\mathrm{eff}})}, \quad Kn^{\mathrm{eff}} = \frac{6D_g}{d_0\bar{v}} \tag{24}$$

The effective Knudsen number Kn^{eff} is defined on the basis of the orifice diameter d_0 instead of the droplet diameter d, whose relation is given by eq 19. However, the physical meaning of Kn^{eff} or eq 24 is not clear.

Precise modeling of the gas-phase transport should take account of (a) purely diffusive transport, (b) gas flow and motion of the droplets, and (c) hydrodynamic interference among the droplets. The last term (c) accounts for the effect that a droplet sweeps the same path in the wake of other droplets. All these factors can be quantitatively treated by computational fluid dynamics (CFD) simulations for the gas flow in the droplet train flow tube.[139,140] The power of this computational technique is that one can straightforwardly evaluate the gas-phase resistance by numerically solving the coupled diffusion and fluid dynamics equations in the flow tube. It is possible for the calculations to mimic accurately the ambient and boundary conditions of experiments.

CFD simulations can be conveniently carried out by a commercial software suite, such as Fluent,[141] and details of CFD simulations are given elsewhere.[122] CFD simulations incorporate uptake of solute species into the droplets by imposing an (incompletely) absorbing boundary condition on the droplet surface. The rate constant of surface deposition k_s is determined from the mass accommodation coefficient α as[122]

$$k_s = \frac{\bar{v}}{2}\frac{\alpha}{2-\alpha} \tag{25}$$

Accordingly, the value of α is treated as an input parameter in the simulation. Then the concentration field of the solute species is calculated in the flow tube, and the uptake coefficient γ is derived via eqs 21−23. The relation between γ and α is thereby unambiguously investigated.

4.4.1. Gas Flow and Concentration—Plug Flow Assumption

CFD simulations can reproduce the solute concentration distribution and the gas flow in the flow tube. Figure 11 illustrates typical examples of radial profiles of concentration and flow velocity. It is apparent in Figure 11a that the solute concentration is strongly depleted near the axis because of uptake into the droplet train. Actually, the concentration gradient of the gas flow is developed cylindrically along the radial direction, implying that the diffusive transport in the flow tube approaches two-dimensional. Figure 11b of the velocity profile shows that the background parabolic profile of laminar flow is perturbed by the moving droplets in the vicinity of the axis.

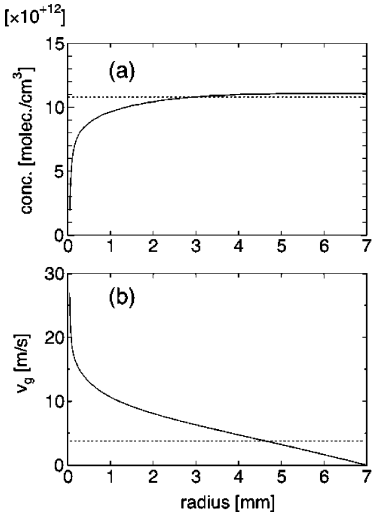

Figure 11. Typical radial profiles of (a) solute concentration and (b) axial gas velocity in the flow tube.[122] The horizontal dotted lines denote the radially averaged values at this cross section. (Reprinted with permission from ref 122. Copyright 2004 American Chemical Society.)

Both radial profiles indicate deviation from plug flow. When the plug flow assumption breaks down in eqs 21−23, the γ value thus derived from the axial concentration decay may not be identical with the value defined from the deposition rate. Here we call the former operational definition of the uptake coefficient "slope γ" (γ_{slope}) and the latter intrinsic definition "local γ" (γ_{local}) to distinguish the two. Estimating the difference between these two quantities is one important goal of CFD simulations.

The difference between γ_{slope} and γ_{local} is partly attributed to the fact that the gas velocity v_g in a nonuniform flow does not necessarily coincide with the solute flow velocity v_{solute}. v_g and v_{solute} are given by

$$v_g = \frac{\int_0^{R_{\mathrm{tube}}} v(r,z)2\pi r\,\mathrm{d}r}{\int_0^{R_{\mathrm{tube}}} 2\pi r\,\mathrm{d}r} = \frac{F_g}{\pi {R_{\mathrm{tube}}}^2} \tag{26}$$

$$v_{\mathrm{solute}} = \frac{\int_0^{R_{\mathrm{tube}}} v(r,z)\,c(r,z)2\pi r\,\mathrm{d}r}{\int_0^{R_{\mathrm{tube}}} c(r,z)2\pi r\,\mathrm{d}r} \tag{27}$$

where $v(r,z)$ and $c(r,z)$ are the axial gas velocity and concentration distributions in the cylindrical coordinates (r,z) and R_{tube} is the radius of the flow tube, as shown in Figure 10. Since $v(r,z)$ and $c(r,z)$ are available from CFD simulations as shown in Figure 11, calculations of v_g and v_{solute} are straightforward at an arbitrary cross section at z. CFD simulations also allow direct evaluation of γ_{local} by calculating the deposition flux into droplets.

Simulations generally yield a tendency for $v_g > v_{\mathrm{solute}}$ and $\gamma_{\mathrm{slope}} > \gamma_{\mathrm{local}}$. The former relation can be anticipated from the gas velocity and concentration profiles of Figure 11, indicating that the axial flow of the solute is mostly carried by background gas flow except near the centerline. Since the gas flow near the centerline is faster than that of the

background because of shear drag by the moving droplets, the solute velocity v_{solute} is generally smaller than the gas velocity v_g. Accordingly, γ_{slope} tends to overestimate the uptake rate, due to F_g ($=v_g\pi R_{tube}^2$) in the denominator of eq 21. Quantitatively speaking, however, it is rather fortunate to have confirmed that the deviation in v_{solute} or γ_{local} is not very significant, within ~10%, for practical conditions of the droplet train apparatus,[122] which supports the conventional analysis of eqs 21−23. The small deviation from plug flow is understood by the fact that the portion of the flow tube under strong perturbation by droplets is restricted to be near the axis and thus its area occupies a relatively small fraction of the cross section of the flow tube.

We also note in passing that the deviation from the plug flow assumption can lead to dramatic consequences when wall loss effects are involved, such as efficient H−D exchange in uptake experiments with isotope exchange, since the wall area is much larger than that of the droplets. In such cases, special care must be taken to derive γ values.[142]

4.4.2. Dependence of Frequency and Speed

Another important assumption in the derivation of γ through eqs 21−23 is that γ_{slope} (and accordingly the gas-phase resistance) does not depend on the orifice frequency f_0 or droplet speed v_d. This assumption is also made in eq 24, the empirical formula for gas-phase resistance in the flow tube. The validity of this dramatically simple assumption is not evident, because these parameters have explicit influence on the droplet configuration and boundary conditions of the gas flow. The validity of this assumption should have a direct consequence on the accuracy of γ and hence α.

The CFD calculations with varying f_0 and v_d have confirmed that the uptake coefficient γ is fairly insensitive to the orifice frequency f_0 or the droplet speed v_d.[139] This approximate invariance of γ with respect to changes in f_0 is valid to within ~15% over the experimental range of f_0. This invariance may be qualitatively understood as follows. By controlling f_0, both the droplet diameter d and spacing d_c vary simultaneously as $d \sim f_0^{-(1/3)}$ and $d_c \sim f_0^{-1}$, indicating that a larger f_0 results in a smaller diameter d and a smaller spacing d_c. Thus, the smaller droplet diameter d reduces the diffusive resistance by increasing the Knudsen number, whereas at the same time the smaller spacing d_c augments the hydrodynamic interference among the train of droplets. These two opposing effects cancel each other to some extent, leading to the apparent invariance.

In terms of the droplet speed dependence, the calculations predicted a tendency for larger values of speed v_d to give larger values of γ. It is quite understandable that droplet movement should facilitate gas transport. The quantitative dependence of γ on v_d turned out to be fairly modest, in parallel to that of the Ranz−Marshall formula.[143] The Ranz−Marshall formula was originally proposed to represent the deposition rate into a single droplet, not a droplet train, under a flow condition. Over the experimental range of v_d (= 16−44 m/s), variation in γ was calculated to be within 11−12% by the CFD calculations.

4.4.3. Quantitative Evaluation for Water Condensation

The CFD simulations have shed light on the uptake process of the droplet train flow tube and, fortunately, have supported some assumptions in current experimental analysis in a semiquantitative sense. The simulation has also revealed that the inherent quantitative accuracy of the conventional experimental analysis is about ~15%. In some cases, the uncertainty in the experimental analysis may have significant consequences on the experimental derivation of α. Here we illustrate a typical and important example, the condensation coefficient of water.

Studies of the water condensation coefficient α have a long history,[30,32,133] though it is still an open question whether α is 1 or not. While condensation and mass accommodation are regarded as the same process at the molecular level, experimental studies of condensation may have additional complicating factors compared to the usual uptake measurements, such as surface impurities or latent heat production during condensation. While it is not straightforward to measure the change in solute concentration during the condensation process, Li *et al.*[33] circumvented this difficulty by employing isotopically labeled water and thereby succeeded in measuring the condensation coefficient using the droplet train flow tube. Their reported value of α is 0.17−0.32 near room temperature, which again is smaller than the value of 1 predicted by MD simulations.[122−125]

The condensation coefficient of water α offers a good opportunity to compare the droplet uptake experiment with molecular simulations, as an example of the accommodation coefficient of soluble species into water. As extensively discussed in section 3, the MD simulations have generally reported a unit sticking probability of water into water near room temperature.[122−125] The mass transfer process of water in experiments is easier to analyze than that of other species because the liquid-phase resistance after condensation, $1/(\Gamma_{sol} + \Gamma_{rxn})$, is thought to be negligible (in fact, finite solubility resistance $1/\Gamma_{sol}$ might play a role in water accommodation into water[144]), allowing us to focus on gas-phase transport and mass accommodation. In this system, the accuracy of $1/\Gamma_g$ is of critical importance to the derivation of α, since the gas-phase transport becomes the rate-determining step. While the gas-phase pressure in the flow tube is much lower than that at atmospheric conditions, the saturated water vapor necessarily imposes a condition of relatively small Knudsen number ($Kn \sim 0.3$ or less) on uptake experiments.

The water uptake process was simulated using CFD simulations under ambient and geometric boundary conditions that precisely correspond to the droplet train experiment. CFD simulations at $T = 0$ °C were performed assuming two values of α, either $\alpha = 0.23$ (experimental value at 0 °C) or $\alpha = 1$ (suggested by the MD result of unit sticking probability[122−125]), and the γ values were derived according to the experimental analysis outlined in section 4.1. Calculated values of γ are compared to experimental ones in Figure 12, plotted as a function of Kn^{eff}. Values computed using the modified Fuchs−Sutugin formula eq 24 overestimate the CFD results for the same value of α. This overestimation is explained by the tendency of the modified Fuchs−Sutugin formula eq 24 to overestimate the gas-phase resistance Γ_g compared to the CFD simulations that accurately mimic the experimental conditions of the water uptake. The lower value of α is needed for the modified Fuchs−Sutugen formula to reproduce the experimental results. The CFD analysis was further utilized to examine the inherent uncertainty in the experimental analysis of water uptake, revealing that the experimental measurement could be interpreted in the range of $\alpha = 0.2-1$ within the current accuracy in the experimental analysis.[122] This implies that the condensation coefficient measured by the droplet train experiment is not necessarily

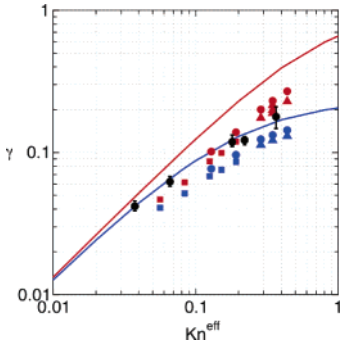

Figure 12. Comparison of simulated and experimental values of γ for water uptake as a function of Kn^{eff}.[122] Red symbols correspond to CFD calculations with an assumed value of $\alpha = 1$, and blue symbols are for CFD calculations with $\alpha = 0.23$, whereas black symbols denote experimental values[33] for $H_2{}^{17}O$. The solid curves denote results using the modified Fuchs−Sutugin formula eq 22 with assumed values of $\alpha = 1$ (red curve) and $\alpha = 0.23$ (blue curve) for α. (Reprinted with permission from ref 122. Copyright 2004 American Chemical Society.)

inconsistent with molecular dynamics simulations. Davidovits *et al.* in their recent comment[103] disagree with this conclusion.

4.5. Summary

While the droplet train apparatus is particularly suitable to study the mass accommodation into water, careful analysis of the gas flow should be a basic requisite for discussing interfacial resistance. The computational fluid dynamics (CFD) calculations are quite useful for this purpose, though the use of CFD is scarce in the field of molecular science. It is rather fortunate that the CFD investigation has justified most of the empirical assumptions routinely used in the experimental analysis semiquantitatively (within ~15%). However, the estimated uncertainty from the CFD simulations also suggests that the empirical formulas should be used with caution when the accurate calibration of the gas-phase resistance is critical, such as for the condensation coefficient of water.

In summary, the relation between the mass accommodation coefficient α, which is derived from heterogeneous kinetic measurements, and the sticking probability α' calculated in molecular simulations remains an open question.[103,144−146] The apparent discrepancy between α and α' challenges the uptake experiments as well as molecular simulations. Precise measurement and analysis of uptake experiments are still challenging, and the current experimental accuracy of these experiments does not necessarily allow for quantitative comparison to molecular simulations in cases of $\alpha > \sim 0.1$. Quantitative understanding of gas-phase and liquid-phase transport should be further pursued as a key to a firm microscopic interpretation of the uptake experiments.

5. Summary and Conclusions

The summary of results from molecular simulations presented in this work supports a picture of solute transport across water's vapor/liquid interface in which a hydrophilic solute molecule impinging on the surface is rapidly equilibrated, sticks to the surface of the interface with nearly unit probability, and then diffuses into the bulk liquid on a free energy surface. Analysis of a large number of experimental observations of uptake, using a variety of techniques, supports a view of mass transport that is diametrically opposed—most solute molecules that collide with the surface return to the vapor rather than being absorbed into the liquid. This discrepancy stresses the need for greater understanding of the important process of uptake.

This work reviewed the results of molecular simulations that were performed with a variety of methods using a large number of interaction potentials. The accuracy of the simulation methods and potentials has been validated for a variety of aqueous properties and processes. However, most of the interaction potentials are empirical (fitted to reproduce experimental data), and interfacial properties were not part of the empirical data used in the fitting procedure. Therefore, the accuracy of these potentials for interfacial processes, particularly those related to uptake, has been recently questioned.[103,145,147] Results from recent X-ray experiments[104,148] have been employed to cast doubt on the accuracy of potentials used in molecular simulations. As discussed in section 3.1, these experimental observations do not provide direct probes of molecular properties calculated in molecular simulations. Complex analysis based upon approximate electronic structure calculations for core−hole excitations is used to extract structural information that is compared with simulation results. The current work presents direct, quantitative comparisons of experimental and computed properties such as surface tension and free energies of solvation and adsorption, and these comparisons provide validation of the accuracy of the potentials used in the simulations. We do not find the qualitative, indirect comparisons cited above a compelling reason to discount the large literature of molecular simulations addressing uptake. In addition, these recent experimental results are not without controversy.[149]

The simulation methods are by necessity approximate. More systematic approaches are now being used to develop interaction potentials for water from first principles, which include important physical effects such as polarization and flexibility (for example, see the work of Xantheas, Burnham, and co-workers[150]). These new potentials have been validated for large water clusters,[151] and as they become validated for bulk water properties, it will be important to test them for interfacial properties to see if they introduce significant changes in any of the important interfacial properties that affect uptake. Another approach would be to modify interaction potentials to reproduce the experimentally derived observation that most incident molecules return to the vapor rather than being solvated. An interesting question is: what types of modifications would be needed to obtain that result and, in doing so, how well would the modified interaction potentials do at reproducing bulk and interfacial properties for which the current interaction potentials do a good job?

Rather than focusing on potential problems with either the molecular simulations or the experiments, for which there is ample evidence that they are adequate, more effort needs to be invested in bridging the gap between the heterogeneous uptake experiments and molecular simulations. As noted in the Introduction, experiments probe macroscopic scales while molecular simulations probe structure and dynamics at microscopic scales. From the experimental side, it is challenging to precisely evaluate the interfacial resistance at the water/vapor interface when the mass accommodation coefficient α is relatively large, typically >0.1. Further work to improve the accuracy of both measurement and analysis is desirable. Some of the key aspects to improve the experimental reliability are quantitative knowledge of the gas-phase and liquid-phase transport, which is in fact lacking under many experimental conditions. Precise description of diffu-

sion and convective flow under realistic boundary conditions should greatly help the analysis of uptake. Then the reliability of the resistance model and the microscopic meaning of the mass accommodation coefficient α will be properly discussed in relation to molecular simulations.

The next step is to go beyond the more phenomenological approaches such as the resistance model to develop multiscale models that accurately include molecular scale phenomena in continuum models. The Boltzmann equation with appropriate boundary conditions provides a means of describing the behavior of vapor phase molecules adjacent to an interface.[152] There has been recent progress in using molecular dynamics simulations to test commonly used forms for kinetic boundary conditions that are employed in the Boltzmann equation.[34,125] Future work that makes a closer connection between a continuum and molecular description may involve extending the Smoluchowski analysis to the Knudsen regime. Analysis based on the Grad analysis of the Boltzmann equation (see for example refs 153 and 154) can take into account some of the molecular details of the interface by extending the analysis to include a potential of mean force profile. The resulting influence on the flux may result in significant deviations from the Fuchs and Sutugin interpolation formula.[129] Further work along these lines, as well as a solution to the Boltzmann equation for conditions relevant to molecular uptake by water surfaces, would be helpful in resolving the current discrepancy between experiment and molecular simulations.

6. Acknowledgments

B.C.G. and G.K.S. would like to thank Drs. Ramona Taylor, Liem Dang, and Douglas Ray for their collaborations and many contributions in this area. A.M. would like to thank Dr. David Hanson, Dr. Masakazu Sugiyama, and Prof. Seiichiro Koda. This work was supported by the Division of Chemical Sciences, Office of Basic Energy Sciences, U.S. Department of Energy. Battelle operates Pacific Northwest National Laboratory for the Department of Energy.

7. References

(1) Seinfeld, J. H.; Pandis, S. N. *Atmospheric Chemistry and Physics of Air Pollution*; Wiley: New York, 1998.

(2) Finlayson-Pitts, B. J.; Pitts, J. N., Jr. *Chemistry of the Upper and Lower Atmosphere*; Academic Press: New York, 2000.

(3) Molina, M. J.; Molina, L. T.; Kolb, C. E. *Annu. Rev. Phys. Chem.* **1996**, *47*, 327.

(4) Reid, J. P.; Sayer, R. M. *Chem. Soc. Rev.* **2003**, *32*, 70.

(5) Goss, K. U. *Crit. Rev. Environ. Sci. Technol.* **2004**, *34*, 339.

(6) George, C.; Ponche, J. L.; Mirabel, P. In *Nucleation and Atmospheric Aerosols*; Fukuta, N., Wagner, P. E., Eds.; Deepak Publishing: Hampton, VA, 1992; p 373.

(7) Kolb, C. E.; Worsnop, D.; Zahniser, M. S.; Davidovits, P.; Keyser, L. F.; Leu, M.-T.; Molina, M. J.; Hanson, D. R.; Ravishankara, A. R.; Williams, L. R.; Tolbert, M. A. In *Progress and Problems in Atmospheric Chemistry*; Barker, J. R., Ed.; World Scientific: Singapore, 1995; p 771.

(8) Nathanson, G. M.; Davidovits, P.; Worsnop, D. R.; Kolb, C. E. *J. Phys. Chem.* **1996**, *100*, 13007. Kolb, C. E.; Davidovits, P.; Jayne, J. T.; Shi, Q.; Worsnop, D. R. *Prog. React. Kinet. Mech.* **2002**, *27*, 1.

(9) Gardner, J. A.; Watson, L. R.; Adewuyi, Y. G.; Davidovits, P.; Zahniser, M. S.; Worsnop, D. R.; Kolb, C. E. *J. Geophys. Res.* **1987**, *92*, 10887. Gardner, J. A.; Watson, L. R.; Adewuyi, Y. G.; Van Doren, J. M.; Davidovits, P.; Worsnop, D. R.; Zahniser, M. S.; Kolb, C. E. *ACS Symp. Ser.* **1989**, *393*, 504. Jayne, J. T.; Gardner, J. A.; Davidovits, P.; Worsnop, D. R.; Zahniser, M. S.; Kolb, C. E. *J. Geophys. Res.* **1990**, *95*, 20559. Jayne, J. T.; Davidovits, P.; Worsnop, D. R.; Zahniser, M. S.; Kolb, C. E. *J. Phys. Chem.* **1990**, *94*, 6041.

(10) Worsnop, D. R.; Zahniser, M. S.; Kolb, C. E.; Gardner, J. A.; Watson, L. R.; Van Doren, J. M.; Jayne, J. T.; Davidovits, P. *J. Phys. Chem.* **1989**, *93*, 1159.

(11) Van Doren, J. M.; Watson, L. R.; Davidovits, P.; Worsnop, D. R.; Zahniser, M. S.; Kolb, C. E. *J. Phys. Chem.* **1990**, *94*, 3265.

(12) Mozurkewich, M.; McMurry, P. H.; Gupta, A.; Calvert, J. G. *J. Geophys. Res.* **1987**, *92*, 4163.

(13) Van Doren, J. M.; Watson, L. R.; Davidovits, P.; Worsnop, D. R.; Zahniser, M. S.; Kolb, C. E. *J. Phys. Chem.* **1991**, *95*, 1684. Bongartz, A.; Kames, J.; Schurath, U.; George, C.; Mirabel, P.; Ponche, J. L. *J. Atmos. Chem.* **1994**, *18*, 149. De Bruyn, W. J.; Swartz, E.; Hu, J. H.; Shorter, J. A.; Davidovits, P.; Worsnop, D. R.; Zahniser, M. S.; Kolb, C. E. *J. Geophys. Res.* **1995**, *100*, 7245. Mertes, S.; Wahner, A. *J. Phys. Chem.* **1995**, *99*, 14000. Poschl, U.; Canagaratna, M.; Jayne, J. T.; Molina, L. T.; Worsnop, D. R.; Kolb, C. E.; Molina, M. J. *J. Phys. Chem. A* **1998**, *102*, 10082. Schweitzer, F.; Magi, L.; Mirabel, P.; George, C. *J. Phys. Chem. A* **1998**, *102*, 593. Swartz, E.; Shi, Q.; Davidovits, P.; Jayne, J. T.; Worsnop, D. R.; Kolb, C. E. *J. Phys. Chem. A* **1999**, *103*, 8824. Boniface, J.; Shi, Q.; Li, Y. Q.; Cheung, J. L.; Rattigan, O. V.; Davidovits, P.; Worsnop, D. R.; Jayne, J. T.; Kolb, C. E. *J. Phys. Chem. A* **2000**, *104*, 7502. Shi, Q.; Davidovits, P.; Jayne, J. T.; Worsnop, D. R.; Kolb, C. E. *J. Phys. Chem. A* **2000**, *104*, 5160. Hanson, D.; Kosciuch, E. *J. Phys. Chem. A* **2003**, *107*, 2199. Tolocka, M. P.; Saul, T. D.; Johnston, M. V. *J. Phys. Chem. A* **2004**, *108*, 2659.

(14) Ponche, J. L.; George, C.; Mirabel, P. *J. Atmos. Chem.* **1993**, *16*, 1.

(15) De Bruyn, W. J.; Shorter, J. A.; Davidovits, P.; Worsnop, D. R.; Zahniser, M. S.; Kolb, C. E. *J. Geophys. Res.* **1994**, *99*, 16927.

(16) Bongartz, A.; Schweighoefer, S.; Roose, C.; Schurath, U. *J. Atmos. Chem.* **1995**, *20*, 35.

(17) Scheer, V.; Frenzel, A.; Behnke, W.; Zetzsch, C.; Magi, L.; George, C.; Mirabel, P. *J. Phys. Chem. A* **1997**, *101*, 9359.

(18) Shi, Q.; Davidovits, P.; Jayne, J. T.; Worsnop, D. R.; Kolb, C. E. *J. Phys. Chem. A* **1999**, *103*, 8812.

(19) Gershenzon, M.; Davidovits, P.; Jayne, J. T.; Kolb, C. E.; Worsnop, D. R. *J. Phys. Chem. A* **2001**, *105*, 7031.

(20) Hanson, D. R.; Burkholder, J. B.; Howard, C. J.; Ravishankara, A. R. *J. Phys. Chem.* **1992**, *96*, 4979.

(21) Magi, L.; Schweitzer, F.; Pallares, C.; Cherif, S.; Mirabel, P.; George, C. *J. Phys. Chem. A* **1997**, *101*, 4943. Muller, B.; Heal, M. R. *Phys. Chem. Chem. Phys.* **2002**, *4*, 3365.

(22) Jayne, J. T.; Duan, S. X.; Davidovits, P.; Worsnop, D. R.; Zahniser, M. S.; Kolb, C. E. *J. Phys. Chem.* **1991**, *95*, 6329.

(23) Jayne, J. T.; Duan, S. X.; Davidovits, P.; Worsnop, D. R.; Zahniser, M. S.; Kolb, C. E. *J. Phys. Chem.* **1992**, *96*, 5452.

(24) Hu, J. H.; Shorter, J. A.; Davidovits, P.; Worsnop, D. R.; Zahniser, M. S.; Kolb, C. E. *J. Phys. Chem.* **1993**, *97*, 11037. Duan, S. X.; Jayne, J. T.; Davidovits, P.; Worsnop, D. R.; Zahniser, M. S.; Kolb, C. E. *J. Phys. Chem.* **1993**, *97*, 2284. Heal, M. R.; Pilling, M. J.; Titcombe, P. E.; Whitaker, B. J. *Geophys. Res. Lett.* **1995**, *22*, 3043. Swartz, E.; Boniface, J.; Tchertkov, I.; Rattigan, O. V.; Robinson, D. V.; Davidovits, P.; Worsnop, D. R.; Jayne, J. T.; Kolb, C. E. *Environ. Sci. Technol.* **1997**, *31*, 2634. Raja, S.; Yaccone, F. S.; Ravikrishna, R.; Valsaraj, K. T. *J. Chem. Eng. Data* **2002**, *47*, 1213. Katrib, Y.; Le Calve, S.; Mirabel, P. *J. Phys. Chem. A* **2003**, *107*, 11433. Raja, S.; Valsaraj, K. T. *J. Air Waste Manage. Assoc.* **2004**, *54*, 1550. Schutze, M.; Herrmann, H. *Phys. Chem. Chem. Phys.* **2004**, *6*, 965. Leyssens, G.; Louis, F.; Sawerysyn, J. P. *J. Phys. Chem. A* **2005**, *109*, 1864.

(25) Jayne, J. T.; Worsnop, D. R.; Kolb, C. E.; Swartz, E.; Davidovits, P. *J. Phys. Chem.* **1996**, *100*, 8015.

(26) Shi, Q.; Li, Y. Q.; Davidovits, P.; Jayne, J. T.; Worsnop, D. R.; Mozurkewich, M.; Kolb, C. E. *J. Phys. Chem. B* **1999**, *103*, 2417.

(27) Katrib, Y.; Mirabel, P.; Le Calve, S.; Weck, G.; Kochanski, E. *J. Phys. Chem. B* **2002**, *106*, 7237.

(28) Muller, B.; Heal, M. R. *J. Phys. Chem. A* **2002**, *106*, 5120.

(29) De Bruyn, W. J.; Shorter, J. A.; Davidovits, P.; Worsnop, D. R.; Zahniser, M. S.; Kolb, C. E. *Environ. Sci. Technol.* **1995**, *29*, 1179. Robinson, G. N.; Worsnop, D. R.; Jayne, J. T.; Kolb, C. E.; Swartz, E.; Davidovits, P. *J. Geophys. Res.* **1998**, *103*, 25371. Takami, A.; Kondo, T.; Kado, A.; Koda, S. *J. Atmos. Chem.* **2001**, *39*, 139.

(30) Mozurkewich, M. *Aerosol Sci. Technol.* **1986**, *5*, 223.

(31) Hagen, D. E.; Schmitt, J.; Trueblood, M.; Carstens, J.; White, D. R.; Alofs, D. J. *J. Atmos. Sci.* **1989**, *46*, 803. Eames, I. W.; Marr, N. J.; Sabir, H. *Int. J. Heat Mass Transfer* **1997**, *40*, 2963. Shaw, R. A.; Lamb, D. *J. Chem. Phys.* **1999**, *111*, 10659. Winkler, P. M.; Vrtala, A.; Wagner, P. E.; Kulmala, M.; Lehtinen, K. E. J.; Vesala, T. *Phys. Rev. Lett.* **2004**, *93*. Davidovits, P.; Worsnop, D. R.; Jayne, J. T.; Kolb, C. E.; Winkler, P.; Vrtala, A.; Wagner, P. E.; Kulmala, M.; Lehtinen, K. E. J.; Vesala, T.; Mozurkewich, M. *Geophys. Res. Lett.* **2004**, *31*. Gershenzon, M.; Davidovits, P.; Williams, L. R.; Shi, Q. A.; Jayne, J. T.; Kolb, C. E.; Worsnop, D. R. *J. Phys. Chem. A* **2004**, *108*, 1567.

(32) Marek, R.; Straub, J. *Int. J. Heat Mass Transfer* **2001**, *44*, 39.
(33) Li, Y. Q.; Davidovits, P.; Shi, Q.; Jayne, J. T.; Kolb, C. E.; Worsnop, D. R. *J. Phys. Chem. A* **2001**, *105*, 10627.
(34) Ishiyama, T.; Yano, T.; Fujikawa, S. *Phys. Rev. Lett.* **2005**, *95*.
(35) Hanson, D. *J. Phys. Chem. B* **1997**, *101*, 4998.
(36) Schwartz, S. E.; Freiberg, J. E. *Atmos. Environ.* **1981**, *15*, 1129.
(37) Schwartz, S. E. In *Chemistry of Multiphase Atmospheric Systems*; Jaeschke, W., Ed.; Springer: Berlin, 1986; Vol. G6, p 415.
(38) Davidovits, P.; Jayne, J. T.; Duan, S. X.; Worsnop, D. R.; Zahniser, M. S.; Kolb, C. E. *J. Phys. Chem.* **1991**, *95*, 6337.
(39) Pohorille, A.; Wilson, M. A. *THEOCHEM* **1993**, *284*, 271.
(40) Benjamin, I. *Accounts Chem. Res.* **1995**, *28*, 233; Pratt, L. R.; Pohorille, A. *Chem. Rev.* **2002**, *102*, 2671.
(41) Stillinger, F. H.; Rahman, A. *J. Chem. Phys.* **1974**, *60*, 1545.
(42) Lemberg, H. L.; Stillinger, F. H. *J. Chem. Phys.* **1975**, *62*, 1677. Rahman, A.; Stillinger, F. H.; Lemberg, H. L. *J. Chem. Phys.* **1975**, *63*, 5223. Stillinger, F. H.; Rahman, A. *J. Chem. Phys.* **1978**, *68*, 666.
(43) Matsuoka, O.; Clementi, E.; Yoshimine, M. *J. Chem. Phys.* **1976**, *64*, 1351. Lie, G. C.; Clementi, E.; Yoshimine, M. *J. Chem. Phys.* **1976**, *64*, 2314.
(44) Jorgensen, W. L.; Chandrasekhar, J.; Madura, J. D.; Impey, R. W.; Klein, M. L. *J. Chem. Phys.* **1983**, *79*, 926.
(45) Carravetta, V.; Clementi, E. *J. Chem. Phys.* **1984**, *81*, 2646.
(46) Berendsen, H. J. C.; Postma, J. P. M.; van Gunsteren, W. F.; Hermans, J. In *Intermolecular Forces*; Pullman, B., Ed.; Reidel: Dordrecht, 1981; p 331. Benjamin, I. *J. Chem. Phys.* **1991**, *95*, 3698.
(47) Berendsen, H. J. C.; Grigera, J. R.; Straatsma, T. P. *J. Phys. Chem.* **1987**, *91*, 6269.
(48) Zhu, S. B.; Fillingim, T. G.; Robinson, G. W. *J. Phys. Chem.* **1991**, *95*, 1002.
(49) Niesar, U.; Corongiu, G.; Huang, M. J.; Dupuis, M.; Clementi, E. *Int. J. Quantum Chem.* **1989**, 421. Niesar, U.; Corongiu, G.; Clementi, E.; Kneller, G. R.; Bhattacharya, D. K. *J. Phys. Chem.* **1990**, *94*, 7949.
(50) Sprik, M.; Klein, M. L. *J. Chem. Phys.* **1988**, *89*, 7556.
(51) Caldwell, J. W.; Kollman, P. A. *J. Phys. Chem.* **1995**, *99*, 6208.
(52) Dang, L. X.; Chang, T. M. *J. Chem. Phys.* **1997**, *106*, 8149.
(53) Car, R.; Parrinello, M. *Phys. Rev. Lett.* **1985**, *55*, 2471.
(54) Vassilev, P.; Hartnig, C.; Koper, M. T. M.; Frechard, F.; van Santen, R. A. *J. Chem. Phys.* **2001**, *115*, 9815. Kuo, I. F. W.; Mundy, C. J. *Science* **2004**, *303*, 658.
(55) Neumann, M. *J. Chem. Phys.* **1985**, *82*, 5663.
(56) Neumann, M. *J. Chem. Phys.* **1986**, *85*, 1567.
(57) Watanabe, K.; Klein, M. L. *Chem. Phys.* **1989**, *131*, 157.
(58) Soetens, J. C.; Costa, M.; Millot, C. *Mol. Phys.* **1998**, *94*, 577.
(59) Benedict, W. S.; Gailar, N.; Plyler, E. K. *J. Phys. Chem.* **1956**, *24*, 1139. Kell, G. S. *J. Chem. Eng. Data* **1975**, *20*, 97. Bertolini, D.; Cassettari, M.; Salvetti, G. *J. Chem. Phys.* **1982**, *76*, 3285.
(60) Matsumoto, M.; Takaoka, Y.; Kataoka, Y. *J. Chem. Phys.* **1993**, *98*, 1464.
(61) Morita, A. *Chem. Phys. Lett.* **2003**, *375*, 1.
(62) Paul, S.; Chandra, A. *Chem. Phys. Lett.* **2004**, *400*, 515.
(63) Tarek, M.; Tobias, D. J.; Klein, M. L. *Physica A* **1996**, *231*, 117. Tarek, M.; Tobias, D. J.; Klein, M. L. *J. Chem. Soc., Faraday Trans.* **1996**, *92*, 559.
(64) Wilson, M. A.; Pohorille, A. *J. Phys. Chem. B* **1997**, *101*, 3130.
(65) Taylor, R. S.; Ray, D.; Garrett, B. C. *J. Phys. Chem. B* **1997**, *101*, 5473.
(66) Taylor, R. S.; Garrett, B. C. *J. Phys. Chem. B* **1999**, *103*, 844.
(67) Shin, J. Y.; Abbott, N. L. *Langmuir* **2001**, *17*, 8434.
(68) Pohorille, A.; Benjamin, I. *J. Chem. Phys.* **1991**, *94*, 5599.
(69) Sokhan, V. P.; Tildesley, D. J. *Faraday Discuss.* **1996**, *104*, 193.
(70) Pohorille, A.; Benjamin, I. *J. Phys. Chem.* **1993**, *97*, 2664.
(71) Benjamin, I. *J. Chem. Phys.* **1999**, *110*, 8070.
(72) Dang, L. X.; Feller, D. *J. Phys. Chem. B* **2000**, *104*, 4403.
(73) Dang, L. X.; Garrett, B. C. *Chem. Phys. Lett.* **2004**, *385*, 309.
(74) Roeselova, M.; Jungwirth, P.; Tobias, D. J.; Gerber, R. B. *J. Phys. Chem. B* **2003**, *107*, 12690.
(75) Roeselova, M.; Vieceli, J.; Dang, L. X.; Garrett, B. C.; Tobias, D. J. *J. Am. Chem. Soc.* **2004**, *126*, 16308.
(76) Vacha, R.; Slavicek, P.; Mucha, M.; Finlayson-Pitts, B. J.; Jungwirth, P. *J. Phys. Chem. A* **2004**, *108*, 11573.
(77) Vieceli, J.; Roeselova, M.; Potter, N.; Dang, L. X.; Garrett, B. C.; Tobias, D. J. *J. Phys. Chem. B* **2005**, *109*, 15876.
(78) Matsumoto, M. *Fluid Phase Equilib.* **1996**, *125*, 195.
(79) Pearlman, D. A.; Case, D. A.; Caldwell, J. C.; Seibel, G. L.; Singh, U. C.; Weiner, P.; Kollman, P. *AMBER*, version 4.0; University of California, San Francisco, 1991.
(80) Brooks, B. R.; Bruccoleri, R. E.; Olafson, B. D.; States, D. J.; Swaminathan, S.; Karplus, M. *J. Comput. Chem.* **1983**, *4*, 187. Mackerell, A. D., Jr.; Brooks, B.; Brooks, C. L., III; Nilsson, L.; Roux, B.; Won, Y.; Karplus, M. In *The Encyclopedia of Computational Chemistry*; Schleyer, P. v. R., Allinger, N. L., Clark, T., Gasteiger, J., Kollman, P. A., Schaefer, H. F., III, Eds.; John Wiley & Sons: Chichester, 1998; Vol. 1, p 271.
(81) Jorgensen, W. L.; Maxwell, D. S.; TiradoRives, J. *J. Am. Chem. Soc.* **1996**, *118*, 11225.
(82) Besler, B. H.; Merz, K. M.; Kollman, P. A. *J. Comput. Chem.* **1990**, *11*, 431.
(83) Allen, M. P.; Tildesley, D. J. *Computer Simulation of Liquids*; Oxford University Press: New York, 1987.
(84) Taylor, R. S.; Dang, L. X.; Garrett, B. C. *J. Phys. Chem.* **1996**, *100*, 11720.
(85) McQuarrie, D. A. *Statistical Mechanics*; Harper and Row: New York, 1976.
(86) Zwanzig, R. W. *J. Chem. Phys.* **1954**, *22*, 1420.
(87) Chandler, D. *Introduction to Modern Statistical Mechanics*; Oxford University Press: New York, 1987.
(88) Penner, S. S. *J. Phys. Chem.* **1952**, *56*, 475. Mortensen, E. M.; Eyring, H. *J. Chem. Phys.* **1960**, *64*, 846.
(89) Wigner, E. *Trans. Faraday Soc.* **1938**, *34*, 29.
(90) Bennett, C. H. In *Diffusion in Solids: Recent Developments*; Burton, J. J., Norwick, A. S., Eds.; Academic Press: New York, 1975; p 73. Bennett, C. H. In *Algorithms for Chemical Computation*; Christofferson, R., Ed.; ACS Symposium Series; American Chemical Society: Washington, DC, 1977. Chandler, D. *J. Chem. Phys.* **1978**, *68*, 2959.
(91) Hynes, J. T. In *Theory of Chemical Reaction Dynamics*; Baer, M., Ed.; CRC Press: Boca Raton, FL, 1985; Vol. IV, p 171.
(92) Schenter, G. K.; Garrett, B. C.; Truhlar, D. G. *J. Chem. Phys.* **2003**, *119*, 5828.
(93) Hynes, J. T. *Annu. Rev. Phys. Chem.* **1985**, *36*, 573.
(94) Kramers, H. A. *Physica (Utrecht)* **1940**, *7*, 284.
(95) Grote, R. T.; Hynes, J. T. *J. Chem. Phys.* **1980**, *73*, 2715.
(96) Townsend, R. M.; Gryko, J.; Rice, S. A. *J. Chem. Phys.* **1985**, *82*, 4391. Wilson, M. A.; Pohorille, A.; Pratt, L. R. *J. Electrochem. Soc.* **1987**, *134*, C505. Wilson, M. A.; Pohorille, A.; Pratt, L. R. *J. Chem. Phys.* **1988**, *88*, 3281. Wilson, M. A.; Pohorille, A.; Pratt, L. R. *J. Chem. Phys.* **1989**, *90*, 5211. Motakabbir, K. A.; Berkowitz, M. L. *Chem. Phys. Lett.* **1991**, *176*, 61. Townsend, R. M.; Rice, S. A. *J. Chem. Phys.* **1991**, *94*, 2207. Benjamin, I. *Phys. Rev. Lett.* **1994**, *73*, 2083.
(97) Wilson, M. A.; Pohorille, A.; Pratt, L. R. *J. Phys. Chem.* **1987**, *91*, 4873.
(98) Matsumoto, M.; Kataoka, Y. *J. Chem. Phys.* **1988**, *88*, 3233.
(99) Lie, G. C.; Grigoras, S.; Dang, L. X.; Yang, D. Y.; McLean, A. D. *J. Chem. Phys.* **1993**, *99*, 3933.
(100) Alejandre, J.; Tildesley, D. J.; Chapela, G. A. *J. Chem. Phys.* **1995**, *102*, 4574.
(101) Du, Q.; Superfine, R.; Freysz, E.; Shen, Y. R. *Phys. Rev. Lett.* **1993**, *70*, 2313. Du, Q.; Freysz, E.; Shen, Y. R. *Science* **1994**, *264*, 826. Richmond, G. L. *Annu. Rev. Phys. Chem.* **2001**, *52*, 357. Richmond, G. L. *Chem. Rev.* **2002**, *102*, 2693.
(102) Morita, A.; Hynes, J. T. *Chem. Phys.* **2000**, *258*, 371.
(103) Davidovits, P.; Worsnop, D. R.; Williams, L. R.; Kolb, C. E.; Gershenzon, M. *J. Phys. Chem. B* **2005**, *109*, 14742.
(104) Wilson, K. R.; Rude, B. S.; Catalano, T.; Schaller, R. D.; Tobin, J. G.; Co, D. T.; Saykally, R. J. *J. Phys. Chem. B* **2001**, *105*, 3346. Wilson, K. R.; Cavalleri, M.; Rude, B. S.; Schaller, R. D.; Nilsson, A.; Pettersson, L. G. M.; Goldman, N.; Catalano, T.; Bozek, J. D.; Saykally, R. J. *J. Phys.: Condens. Matter* **2002**, *14*, L221. Wilson, K. R.; Schaller, R. D.; Co, D. T.; Saykally, R. J.; Rude, B. S.; Catalano, T.; Bozek, J. D. *J. Chem. Phys.* **2002**, *117*, 7738.
(105) MacRitchie, F. *Chemistry at Interfaces*; Academic Press: New York, 1990.
(106) Lee, C. Y.; Scott, H. L. *J. Chem. Phys.* **1980**, *73*, 4591.
(107) Paul, S.; Chandra, A. *Chem. Phys. Lett.* **2003**, *373*, 87.
(108) Vieceli, J.; Roeselova, M.; Tobias, D. J. *Chem. Phys. Lett.* **2004**, *393*, 249.
(109) Braslau, A.; Deutsch, M.; Pershan, P. S.; Weiss, A. H.; Alsnielsen, J.; Bohr, J. *Phys. Rev. Lett.* **1985**, *54*, 114. Braslau, A.; Pershan, P. S.; Swislow, G.; Ocko, B. M.; Alsnielsen, J. *Phys. Rev. A* **1988**, *38*, 2457.
(110) Pratt, L. R. *J. Phys. Chem.* **1992**, *96*, 25.
(111) Kuzmin, V. L.; Brodskaya, E. N. *Colloid J.* **1995**, *57*, 776. Dang, L. X.; Chang, T. M. *J. Phys. Chem. B* **2002**, *106*, 235.
(112) Sokhan, V. P.; Tildesley, D. J. *Mol. Phys.* **1997**, *92*, 625.
(113) Paluch, M. *Adv. Colloid Interface Sci.* **2000**, *84*, 27; Parfenyuk, V. I. *Colloid J.* **2002**, *64*, 588.
(114) Ben-Naim, A.; Marcus, Y. *J. Chem. Phys.* **1984**, *81*, 2016.
(115) Karpovich, D. S.; Ray, D. *J. Phys. Chem. B* **1998**, *102*, 649.
(116) Sander, R., 1999, URL: http://www.mpch-mainz.mpg.de/sander/res/henry.html.
(117) Autrey, T.; Brown, A. K.; Camaioni, D. M.; Dupuis, M.; Foster, N. S.; Getty, A. *J. Am. Chem. Soc.* **2004**, *126*, 3680.

(118) Castro, A.; Bhattacharyya, K.; Eisenthal, K. B. *J. Chem. Phys.* **1991**, *95*, 1310.
(119) Dabkowski, J.; Zagorska, I.; Dabkowska, M.; Koczorowski, Z.; Trasatti, S. *J. Chem. Soc., Faraday Trans.* **1996**, *92*, 3873.
(120) Allen, H. C.; Gragson, D. E.; Richmond, G. L. *J. Phys. Chem. B* **1999**, *103*, 660.
(121) Morita, A.; Kanaya, Y.; Francisco, J. S. *J. Geophys. Res.* **2004**, *109*, D09201.
(122) Morita, A.; Sugiyama, M.; Kameda, H.; Koda, S.; Hanson, D. R. *J. Phys. Chem. B* **2004**, *108*, 9111.
(123) Nagayama, G.; Tsuruta, T. *J. Chem. Phys.* **2003**, *118*, 1392.
(124) Tsuruta, T.; Nagayama, G. *J. Phys. Chem. B* **2004**, *108*, 1736.
(125) Ishiyama, T.; Yano, T.; Fujikawa, S. *Phys. Fluids* **2004**, *16*, 4713.
(126) Berne, B. J.; Borkovec, M.; Straub, J. E. *J. Phys. Chem.* **1988**, *92*, 3711. Woolf, T. B.; Roux, B. *J. Am. Chem. Soc.* **1994**, *116*, 5916. Wick, C. D.; Dang, L. X. *J. Phys. Chem. B* **2005**, *109*, 15574.
(127) Johnson, D. O.; Stebe, K. J. *J. Colloid Interface Sci.* **1996**, *182*, 526.
(128) Davidovits, P.; Hu, J. H.; Worsnop, D. R.; Zahniser, M. S.; Kolb, C. E. *Faraday Discuss.* **1995**, *100*, 65.
(129) Fuchs, N. A.; Sutugin, A. G. *Highly Dispersed Aerosols*; Ann Arbor Science Publishers: Ann Arbor, MI, 1970.
(130) Smoluchowski, M. *Phys. Chem.* **1918**, *92*, 129; Collins, F. C.; Kimball, G. E. *J. Colloid Sci.* **1949**, *4*, 425.
(131) Motz, H.; Wise, J. *J. Chem. Phys.* **1960**, *32*, 1893.
(132) Danckwerts, P. V. *Gas−Liquid Reactions*; McGraw-Hill: New York, 1970.
(133) Pruppacher, H. R.; Klett, J. D. *Microphysics of Clouds and Precipitation*; Kluwer Academic Publishers: Boston, 1997.
(134) Vesala, T.; Hannemann, A. U.; Luo, B. P.; Kulmala, M.; Peter, T. *J. Aerosol. Sci.* **2001**, *32*, 843.
(135) Kulmala, M.; Wagner, P. E. *J. Aerosol. Sci.* **2001**, *32*, 833.
(136) Widmann, J. F.; Davis, E. J. *J. Aerosol. Sci.* **1997**, *28*, 1233.
(137) Baboolal, L. B.; Pruppacher, H. R.; Topalian, J. H. *J. Atmos. Sci.* **1981**, *38*, 856.
(138) Worsnop, D. R.; Shi, Q.; Jayne, J. T.; Kolb, C. E.; Swartz, E.; Davidovits, P. *J. Aerosol. Sci.* **2001**, *32*, 877.
(139) Morita, A.; Sugiyama, M.; Koda, S. *J. Phys. Chem. A* **2003**, *107*, 1749.
(140) Sugiyama, M.; Koda, S.; Morita, A. *Chem. Phys. Lett.* **2002**, *362*, 56.
(141) *FLUENT*, version 6; Fluent, Inc.: Lebanon, NH, http://www.fluent-.com/.
(142) Hanson, D. R.; Sugiyama, M.; Morita, A. *J. Phys. Chem. A* **2004**, *108*, 3739.
(143) Ranz, W. E.; Marshall, W. R. *Chem. Eng. Prog.* **1952**, *48*, 141.
(144) Morita, A.; Sugiyama, M.; Koda, S.; Hanson, D. R. *J. Phys. Chem. B* **2005**, *109*, 14747.
(145) Worsnop, D. R.; Williams, L. R.; Kolb, C. E.; Mozurkewich, M.; Gershenzon, M.; Davidovits, P. *J. Phys. Chem. A* **2004**, *108*, 8542.
(146) Morita, A.; Sugiyama, M.; Koda, S. *J. Phys. Chem. A* **2004**, *108*, 8544.
(147) Worsnop, D. R.; Williams, L. R.; Kolb, C. E.; Mozurkewich, M.; Gershenzon, M.; Davidovits, P. *J. Phys. Chem. A* **2004**, *108*, 8546.
(148) Wernet, P.; Nordlund, D.; Bergmann, U.; Cavalleri, M.; Odelius, M.; Ogasawara, H.; Naslund, L. A.; Hirsch, T. K.; Ojamae, L.; Glatzel, P.; Pettersson, L. G. M.; Nilsson, A. *Science* **2004**, *304*, 995.
(149) Smith, J. D.; Cappa, C. D.; Wilson, K. R.; Messer, B. M.; Cohen, R. C.; Saykally, R. J. *Science* **2004**, *306*, 851. Nilsson, A.; Wernet, P.; Nordlund, D.; Bergmann, U.; Cavalleri, M.; Odelius, M.; Ogasawara, H.; Naslund, L. A.; Hirsch, T. K.; Glatzel, P.; Pettersson, L. G. M. *Science* **2005**, *308*, 793a. Smith, J. D.; Cappa, C. D.; Messer, B. M.; Cohen, R. C.; Saykally, R. J. *Science* **2005**, *308*, 793b.
(150) Burnham, C. J.; Xantheas, S. S. *J. Chem. Phys.* **2002**, *116*, 5115. Burnham, C. J.; Xantheas, S. S. *J. Chem. Phys.* **2002**, *116*, 1500. Xantheas, S. S.; Burnham, C. J.; Harrison, R. J. *J. Chem. Phys.* **2002**, *116*, 1493. Burnham, C. J.; Xantheas, S. S. *J. Chem. Phys.* **2002**, *116*, 1479.
(151) Fanourgakis, G. S.; Apra, E.; Xantheas, S. S. *J. Chem. Phys.* **2004**, *121*, 2655. Fanourgakis, G. S.; Apra, E.; de Jong, W. A.; Xantheas, S. S. *J. Chem. Phys.* **2005**, *122*.
(152) Cercignani, C. *Rarefied Gas Dynamics*; Cambridge University Press: New York, 2000. Sone, Y. *Kinetic theory and Fluid Dynamics*; Birkhäuser: Boston, 2002.
(153) Qu, X.; Davis, E. J. *J. Aerosol. Sci.* **2001**, *32*, 861. Qu, X.; Davis, E. J.; Swanson, B. D. *J. Aerosol.* Sci. **2001**, *32*, 1315.
(154) Sitarski, M.; Nowakowski, B. *J. Colloid Interface Sci.* **1979**, *72*, 113.
(155) Sprik, M. *J. Chem. Phys.* **1991**, *95*, 6762.

CR040370W